Heliyon 10 (2024) e30983

Contents lists available at ScienceDirect

Heliyon

journal homepage: www.cell.com/heliyon

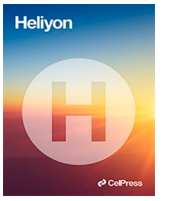

Research article

Revealing the potential bioactive components and mechanism of Qianhua Gout Capsules in the treatment of gouty arthritis through network pharmacology, molecular docking and pharmacodynamic study strategies

Gelin Xiang [a,b,1], Luyin Yang [a,d,1], Jing Qin [b], Shaohui Wang [b,c,***], Yi Zhang [b,c,**], Sijin Yang [a,d,*]

[a] National Traditional Chinese Medicine Clinical Research Base and Drug Research Center of the Affiliated Traditional Chinese Medicine Hospital of Southwest Medical University, Luzhou, China
[b] State Key Laboratory of Southwestern Chinese Medicine Resources, School of Ethnic Medicine of Chengdu University of Traditional Chinese Medicine, Chengdu, China
[c] Meishan Hospital of Chengdu University of Traditional Chinese Medicine, Meishan, China
[d] Institute of Integrated Chinese and Western Medicine, Southwest Medical University, Luzhou, China

ARTICLE INFO

Keywords:
Qianhua gout capsules
Gouty arthritis
UPLC-Q exactive-MS
Network pharmacology
Molecular docking

ABSTRACT

Recent clinical studies have confirmed the effectiveness of Qianhua Gout Capsules (QGC) in the treatment of gouty arthritis (GA). However, the specific regulatory targets and mechanisms of action of QGC are still unclear. To address this gap, we utilized network pharmacology, molecular docking, and pharmacodynamic approaches to investigate the bioactive components and associated mechanisms of QGC in the treatment of GA. By employing UPLC-Q Exactive-MS, we identified the compounds present in QGC, with active ingredients defined as those with oral bioavailability ≥30 % and drug similarity ≥0.18. Subsequently, the targets of these active compounds were determined using the TCMSP database, while GA-related targets were identified from DisGeNET, GeneCards, TTD, OMIM, and DrugBank databases. Further analysis including PPI analysis, GO analysis, and KEGG pathway enrichment was conducted on the targets. Validation of the predicted results was performed using a GA rat model, evaluating pathological changes, inflammatory markers, and pathway protein expression. Our results revealed a total of 130 components, 44 active components, 16 potential shared targets, GO-enriched terms, and 47 signaling pathways related to disease targets. Key active ingredients included quercetin, kaempferol, β-sitosterol, luteolin, and wogonin. The PPI analysis highlighted five targets (PPARG, IL-6, MMP-9, IL-1β, CXCL-8) with the highest connectivity, predominantly enriched in the IL-17 signaling pathway. Molecular docking experiments demonstrated strong binding of CXCL8, IL-1β, IL-6,

* Corresponding author. National Traditional Chinese Medicine Clinical Research Base and Drug Research Center of the Affiliated Traditional Chinese Medicine Hospital of Southwest Medical University, No.182, Chunhui Road, Longmatan District, Luzhou, China.
** Corresponding author. State Key Laboratory of Southwestern Chinese Medicine Resources, Chengdu University of Traditional Chinese Medicine, 1166 Liutai Avenue, Wenjiang District, Chengdu, China.
*** Corresponding author. State Key Laboratory of Southwestern Chinese Medicine Resources, School of Ethnic Medicine of Chengdu University of Traditional Chinese Medicine, Chengdu, China.
E-mail addresses: winter9091@163.com (S. Wang), zhangyi@cdutcm.edu.cn (Y. Zhang), ysjimn@sina.com (S. Yang).
[1] These authors contributed to this work equally.

https://doi.org/10.1016/j.heliyon.2024.e30983
Received 8 January 2024; Received in revised form 8 May 2024; Accepted 8 May 2024
Available online 10 May 2024

MMP9, and PPARG targets with the top five active compounds. Furthermore, animal experiments confirmed the efficacy of QGC in treating GA in rats, showing reductions in TNF-α, IL-6, and MDA levels, and increases in SOD levels in serum. In synovial tissues, QGC treatment upregulated CXCL8 and PPARG expression, while downregulating IL-1β, MMP9, and IL-6 expression. In conclusion, this study applied a network pharmacology approach to uncover the composition of QGC, predict its pharmacological interactions, and demonstrate its *in vivo* efficacy, providing insights into the anti-GA mechanisms of QGC. These findings pave the way for future investigations into the therapeutic mechanisms underlying QGC's effectiveness in the treatment of GA.

Abbreviations

Akt	Protein Kinase B
BP	Biological Process
CC	Cellular Component
C-EBP	CCAAT-Enhancer Binding Protein
CXCL8	C-X-C Motif Chemokine Ligand 8
DL	Drug Likeness score
ESI	Electrospray Ion Source
FOXP3	Recombinant Forkhead Box P3
GA	Gouty Arthritis
GO	Kyoto Gene Ontology
IL-1β	Human IL-1 Beta Protein
IL-4	Interleukin-4
IL-5	Interleukin-5
IL-6	Interleukin 6
IL-17	Interleukin 17
IOD	Integrated Optical Density
KEGG	Kyoto Encyclopedia of Genes and Gnomes
MAPK	Mitogen Activated Protein Kinase
MDA	Malondialdehyde
MetS	Metabolic Syndrome
MF	Molecular Function
MMP-9	Matrix Metallo Protein 9
MSU	Monosodium Urate
NF-κB	Nuclear Factor kappa-B
NSAIDs	non-steroidal anti-inflammatory drugs
OB	Oral Bioavailability
OMIM	Online Mendelian Inheritance in Man
PGP	Prolyl-Glycyl-Proline
PI3K	Phosphatidylinositide 3 Kinases
PPARG	Peroxisome Proliferator Activated Receptor Gamma
PPI	Protein-protein interaction
QGC	Qianhua Gout Capsule
STAT3	Signal Transducer and Activator of Transcription 3
SOD	Superoxide Dismutase
TCMSP	Traditional Chinese Medicine Systems Pharmacology Database and Analysis Platform
TNF-α	Tumor Necrosis Factor Alpha
TTD	Therapeutic Target Database

1. Introduction

Gouty arthritis (GA) is a condition characterized by the excessive deposition of monosodium urate crystals in various tissues, leading to local tissue damage and inflammation. This dysfunction in purine metabolism is the underlying cause of GA [1]. Common symptoms of GA include painful swelling and limited mobility in joints like the knee, ankle, toe, and fingers, with a hereditary component [2]. In Chinese medicine, gout is referred to as "Li Jie", "paralysis", and "Gout", while modern medicine classifies it as "Zuo

Tan" and "Gao Bing" [3]. GA is a prevalent and recurring disease in society, presenting challenges to patients' well-being [4]. Current drugs for GA, such as non-steroidal anti-inflammatory drugs (NSAIDs) and uric acid inhibitors, can have adverse effects like liver and kidney damage or gastrointestinal reactions [5,6]. Chinese medicine offers a promising alternative with low side-effects and multi-targeted therapeutic properties, making it crucial to explore as a treatment option for GA.

The Qianhua Gout Capsules (QGC) prescription is based on the traditional recipe of Luzhou Baihui Zhishen Pharmaceutical Technology Co., Ltd. This formula, used to treat gouty arthritis (GA), includes Rubiae Radix et Rhizoma (Qian Cao), Zanthoxyli Pericarpium (Hua Jiao), Tetrapanacis Medulla (Tong Cao), and *Liparis nervosa* (Thunb.) Lindl. (Jian Xue Qing). QGC is known for its effectiveness in cooling blood, dissipating blood stasis, clearing collaterals, alleviating pain, and relieving heat and urine retention [7,8]. It is commonly used for symptoms like redness, swelling, heat, pain, and numbness in joints or muscles due to GA [9]. Despite its widespread use and positive feedback from both physicians and patients [9,10], the specific active ingredients and mechanisms responsible for its efficacy remain unclear.

With the rapid advancement of bioinformatics and big data, the research approach of systems pharmacology has become increasingly sophisticated. Systems pharmacology, a term coined in recent years, represents an emerging interdisciplinary field that integrates experimental validation with computational tools (such as web-based bioinformatics analysis, pharmacology, and molecular biology techniques). This approach offers effective strategies for elucidating the active compounds and potential mechanisms implicated in the treatment of gastric ulcers with Qinggan Qingre Chubi (QGC) [11,12]. In this study, we applied a systems pharmacology methodology that incorporates network pharmacology, molecular docking, and pharmacodynamic investigations to comprehensively explore the potential active components and mechanisms of action of QGC in gastric ulcer treatment. Initially, we conducted an analysis of the chemical constituents in QGC utilizing UPLC-Q Exactive-MS. Subsequently, we employed network pharmacology and molecular docking techniques to predict the potential active compounds, targets, and pathways involved in the treatment of gastric ulcers with QGC. Finally, we validated the therapeutic mechanism of QGC in gastric ulcers using a rat model (Fig. 1). These findings offer both theoretical insights and practical implications for the clinical utilization of QGC.

2. Materials and methods

2.1. Materials

2.1.1. Instrument

Vanquish ultra-high performance liquid chromatography coupled with Q-Exactive quadrupole-electrostatic field orbital hydrazine high-resolution mass spectrometer (Thermo Fisher Scientific, USA), SB-8200DTS dual-frequency ultrasound instrument (frequency 40 kHz, power 650 W, Ningbo Xingyi Ultrasonic Equipment Co., Ltd.), BSA124S one-hundred-thousandth electronic analytical balance (Sartorius Scientific Instruments Co., Ltd.), FA1004 one-millionth electronic analytical balance (Shanghai Liangping Instrument Co.,

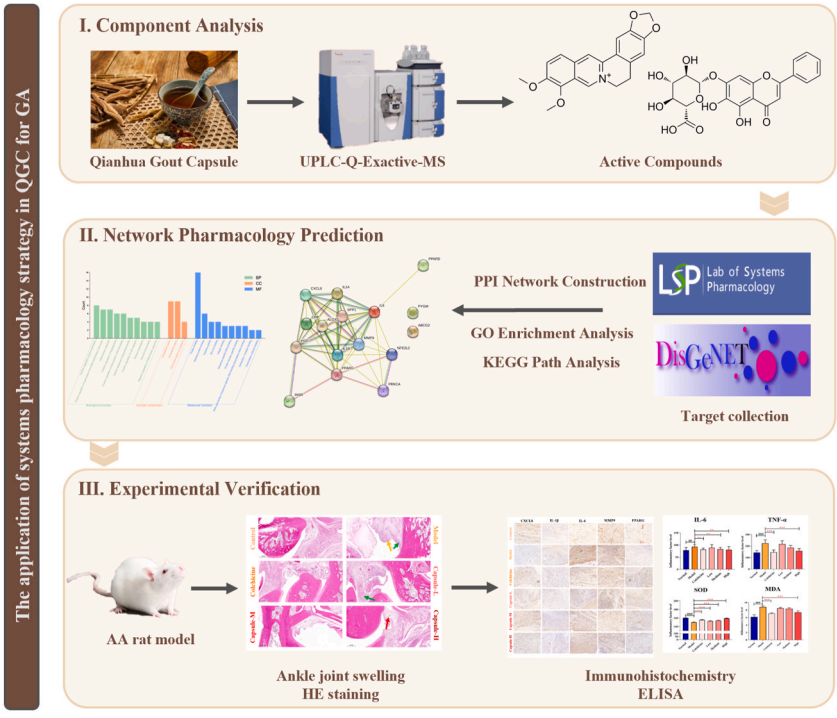

Fig. 1. The working flow chart of the current study.

Ltd.), Varioskan Flash full-wavelength multifunctional enzyme standard, STP420 ES fast tissue dehydrator, HM325 microtome, Varistain™ Gemini ES automatic dyeing machine, Autostainer 360 fully automated glass slipper, PrintMate AS embedding box marking machine (Thermo Fisher Scientific, USA), JB-P5 embedding machine, JB-L5 freezing table, JXL-818 wax repair instrument, JK-6 tissue spreading and baking machine (Wuhan Junjie Electronics Co., Ltd.), DHG-9240A electric blast drying oven (Shanghai Yiheng Scientific Instrument Co., Ltd.), and slide and cover glass (Jiangsu Shitai Experimental Equipment Co., Ltd.).

2.1.2. Reagents

The chromatography grade acetonitrile and chromatography grade formic acid (Fisher, Inc., USA), Watson's distilled water (Watson's Trademark Co., Ltd.), interleukin-6 ELISA kit (IL-6, batch No.: MM-3660302), tumor necrosis factor-α ELISA kit (TNF-α, batch number: MM-160002), superoxide dismutase kit (SOD, Nanjing Jiancheng Bioengineering Research Institute, batch number: 200221008, article number: A001-1-2), and malondialdehyde determination kit (MDA, Nanjing Jiancheng Bioengineering Research Institute, batch number: 200221011, article number: A003-1-2).

2.1.3. Animals

Male SPF grade SD rats were sourced from Chengdu Enswell Biotechnology Co. under production license SCXK (Xiang) 2019-0004. The animals were housed in both shielded and open systems at the Experimental Animal Center of Chengdu University of TCM Innovation Research Institute, Sichuan Province, with the laboratory designation TCM-09-315. Each rat was kept in an individual cage with access to food and water, and bedding was changed regularly. The rats were maintained at a temperature range of 20–24 °C and a humidity level of 40%–60 %, while being exposed to a 12/12 h light and dark cycle.

2.1.4. Chemical standards

QGC (provided by the laboratory of Affiliated Hospital of Southwest Medical University). Sodium Uric Acid Crystals (5 g, Rohn Reagent, Lot No. RH389360). Colchicine (100 mg/stem, Rohn Reagent, Lot No. RH341403). Maltol (Purity ≥98 %, Sichuan Weikeqi Biological Technology Co.,Ltd., Lot No. wkq22070114). Cafferic acid (Purity >98 %, Ltd , Lot No. DSTDE001301) and Catechin (Purity >99.87 %, Lot No. DSTDE000102) are from Chengdu Desite Biotechnology Co., Ltd. β-Sitosterol (Purity >98 %, Chengdu Ruifensidan Biotechnology Co., Ltd, Lot No. G00202005008), Ferulic acid (Lot No. RFS-A00211812016), Luteolin (Lot No. RFS-M00702004028), Baicalin (Lot No. RFS-H01811804026), Berberine (Lot No. RFS-Y03511811015), Quercetine (Lot No. RFS-H00911812016), Apigenin (Lot No. RFS-Q00211801029), Isorhamnetin (Lot No. RFS-Y03911811003) and Tangeritin (Lot No. RFS-J02202008018) all have purity >98 %, which were from Chengdu Herbpurify Co., Ltd. Kaempferol (Purity >98 %, Lot No. MSUT-13121112) and Neochlorogenic acid (Purity >99.40 %, Lot No. MSUT-21070910) were from Chengdu MUST Bio-Technology Co., Ltd. Mollugin (Purity >99.90 %, Chengdu MUST Bio-Technology Co., Ltd, Lot No. MSUT-21060211).

2.1.5. Preparation of the test solution

Precisely measured 2.00 g of QGC sample was placed in a stoppered conical flask, followed by the addition of 25 mL of methanol to the flask which was then tightly stoppered. The flask was weighed again before being subjected to ultrasonication for 30 min at 250 W and 40 kHz. After cooling, the flask was weighed once more. Methanol was added to compensate for any weight loss, the flask was shaken well, and the contents were filtered through a 0.22 μm microporous filtration membrane. The filtrate was collected as the final product.

2.2. Chromatographic and mass spectrometric conditions

2.2.1. Chromatographic conditions

The study utilized a Thermo Scientific AccucoreTM C18 column measuring 3 mm × 100 mm with a particle size of 2.6 μm. The mobile phase comprised 0.1 % formic acid water (A) and 0.1 % formic acid acetonitrile (B), with a gradient elution ranging from 10 % to 95 % B over a period of 0–40 min, followed by a constant 95 % B from 40 to 45 min. The flow rate was maintained at 0.2 mL/min, and the column temperature was set at 30 °C. An injection volume of 5 μL was used.

2.2.2. Mass spectrometry conditions

An Electrospray ion source (ESI) was used for detecting positive/negative ions. The spray voltage was 3.2 kV, and the ion source temperature was kept at 350 °C. The sheath gas flow rate was 35 arbitrary units (arb), with the auxiliary gas flow rate set at 10 arb. Additionally, the ion transport tube temperature was 320 °C. The scan mode utilized was full scan/data-dependent secondary scan (Full MS/dd-MS2) with a primary resolution of 70,000 and a secondary resolution of 17,500. The scan range covered m/z 100–1500. It is important to note that nitrogen was the gas used throughout the experiment.

2.3. Collection of chemical components and GA related targets of QGC

2.3.1. Collection of active ingredients related targets

The composition structure of QGC was analyzed using the TCM Systems Pharmacology Database and Analysis Platform (TCMSP, https://www.tcmsp-e.com/tcmsp.php) with mass spectrometry as keywords for searching. Active ingredients of QGC were filtered based on oral bioavailability (OB) ≥ 30 % and drug likeness score (DL) ≥ 0.18. The compounds were then validated twice using the bioinformatics analysis platform BATMAN-TCM (http://bionet.ncpsb.org/batman-tcm/) with a minimum structural similarity score of

20.

2.3.2. Gene annotation of relevant targets of QGC

The UniProt database, also known as the protein database, contains a wealth of annotation information and protein sequence data. In the TCMSP database, the target protein corresponding to the active ingredients was identified and matched with proteins in UniProt to obtain the standardized gene name linked to the protein, representing the target gene of QGC. The active ingredients and targets identified were then input into Cytoscape 3.9.1 software to construct a network of drug active ingredient-targets. The network analyzer function was utilized to analyze network characteristics and predict node importance based on their degrees.

2.3.3. Collection of GA related targets

To identify GA-related targets, we conducted a thorough search using the DisGeNET database (https://disgenet.org/) with GA as a keyword. Additionally, we supplemented our search by utilizing GeneCards (https://www.genecards.org/), Therapeutic Target Database (TTD, db.idrblab.net/ttd/), DrugBank (https://go.drugbank.com/), Online Mendelian Inheritance in Man (OMIM, https://www.omim.org/), and other relevant databases. The identified targets were then converted into standardized gene names using the Uniport database.

2.3.4. Screening for "disease-drug" intersection targets using Venn diagrams

The VENNY 2.1 online tool was utilized to compare the active ingredient genes obtained from section 2.3.1 with the gout disease genes obtained from section 2.3.3. By constructing a Venn diagram, the common genes between the drug and disease, referred to as intersection genes, were identified. These intersection genes represent the target genes for linking the active ingredient to gout disease, potentially playing a significant role in treatment. Subsequently, a network named 'drug-active ingredient-disease target-GA' was created using Cytoscape 3.9.1 software. The network analyzer function was then used to analyze the network and predict the treatment node based on the degree value.

2.3.5. Construction of PPI network construction

Protein-protein interaction (PPI) networks were constructed using the STRING online software database (https://string-db.org/) with "*Homo sapiens*" and "medium-medium confidence (0.400)" as parameters. The data on node1, node2, and Combine Score was then imported into Cytoscape 3.9.1 software for visualization and network analysis.

2.3.6. GO and KEGG pathway analysis

The intersecting genes were analyzed for biological process enrichment using Gene Ontology (GO) and pathway enrichment using Kyoto Encyclopedia of Genes and Genomes (KEGG) via the CluoGo plug-in in Cytoscape 3.9.1 software. The analysis was conducted on *Homo sapiens* species, with a threshold value of $p < 0.05$ applied. The resulting data was visualized using bar graphs on the microbiotope online mapping website (http://www.bioinformatics.com.cn/).

2.4. Molecular docking

The compound structural formulae were retrieved from TCMSP, Pubchem, and other databases, and saved in mol2 format. The 3D structures of receptor proteins were obtained from the PDB protein database. These structures were screened using X-ray structure analysis and Å-value criteria, and subsequently downloaded and stored in PDB format. Molecular docking simulations were conducted using the Cavity-detection guided Blind Docking (CB-DOCK2) online analysis platform (https://cadd.labshare.cn/cb-dock2/php/index.php). The results of the analysis and corresponding molecular docking maps were compiled and saved for future reference.

2.5. Animal model validation of QGC anti-GA mechanism

2.5.1. Grouping and drug administration

Thirty-six male Sprague-Dawley rats were divided into six groups: a normal group, a model group, a positive drug group (colchicine, 0.2 mg/kg), and three QGC dose groups (low-dose 95 mg/kg, medium-dose 190 mg/kg, high-dose 378 mg/kg), each consisting of six rats. The dosages administered to the rats were determined based on preliminary experiments conducted by the research team [10]. The dosage calculation was performed using the equivalent dose coefficient discounting method, with a daily dose equivalent to 1.8 g for humans [13]. The volume of administration was calculated based on 10 mL/kg and the rats' mass prior to each administration. The drug was orally administered once daily for a period of 14 days. The blank and model groups were given an equal volume of saline daily, and the model was induced after 12 days of administration while continuing the drug.

2.5.2. Model building and sample collection

Isoflurane was administered for approximately 5 s to induce general anesthesia. Subsequently, a 0.2 mL MSU particles suspension (2.5 g/100 mL) was injected into the joint cavity of the rat's right ankle joint using a sterilized 1 mL syringe needle. The injection was performed at a 45° angle to the medial side of the tibial tendon, with the contralateral bulge confirming successful modeling of GA. In contrast, the normal group received a 0.2 mL saline injection. The groups receiving colchicine and QGC were orally administered their respective original doses 1 h after establishing the model. Relevant symptoms and indexes were observed 48 h after model establishment. Following the experiment, the rats were intraperitoneally injected with hydrofluoric acid (350 mg/kg). Blood samples were

then collected from the abdominal aorta after anesthesia, and the supernatant was obtained by centrifugation at 3500 r/min for 10 min.

2.5.3. Change in ankle joint swelling

Following the injection of MSU solution or an equivalent volume of saline into the right hind ankle joint, the contralateral swollen joint was identified with a black marker for subsequent measurement and positioning. The diameter of the marked joint was assessed using a digital vernier caliper at 0 h (baseline), as well as at 0, 2, 4, 8, and 24 h post-injection. Each measurement was performed thrice, and the average value was calculated to ascertain the extent of swelling. The degree of swelling was determined by the formula: Swelling = (joint diameter at a specific time point post-injection - joint diameter at baseline)/joint diameter at baseline × 100 %.

2.5.4. Histopathological observation

After blood collection, the tibio-tarsal joint of the right hind foot was meticulously dissected, preserving approximately 0.5 cm of the proximal and distal ends of the joint. The dissected joint underwent standard processing and paraffin embedding. Sections were then prepared for the analysis of pathological changes in the synovial tissue of rats using Hematoxylin and Eosin (HE) staining. Each section was examined at a 50× magnification to identify any general lesions. Images were captured at 100× and 400× magnifications from specific areas of interest, and were subsequently analyzed according to the criteria outlined in Table 1.

2.5.5. ELISA assay

Serum levels of IL-6 and TNF-α were quantified using an ELISA assay. The expression levels of SOD and MDA were assessed following the protocols outlined in the respective kits.

2.5.6. Immunohistochemistry

To validate the predicted results obtained from network pharmacology, we performed immunohistochemical staining using antibodies from Bioss (Beijing, China) to detect IL-6, PPARG, IL-1β, MMP-9, and CXCL-8. Quantitative analysis of each marker was conducted with the Image-Pro Plus 6.0 software suite, measuring the integrated optical density (IOD) of stained regions in the micrographs. It is important to highlight that higher IOD values directly indicate higher levels of marker expression.

2.5.7. Statistical methods

The statistical analysis was performed using SPSS 19.0 software. The data was expressed as mean ± standard deviation ($\bar{x} \pm s$). The sample means of each group were analyzed using chi-square test and one-way ANOVA. A p-value below 0.05 was deemed statistically significant.

3. Results

3.1. Analysis of chemical composition of QGC

The extracts of QGC were sampled and analyzed using liquid-phase mass spectrometry. The analysis identified 130 compounds in QGC, including 4 amino acids, 9 polyphenols, 3 nucleosides and their bases, 20 flavonoids, 3 coumarins, 29 organic acids, 9 alkaloids, 2 sugars, 4 anthraquinones, 4 quinones, 5 terpenoids, 4 amides, 6 sterols, and 28 other compounds. Fig. 2 illustrates the total ion flow diagrams of the test articles in positive and negative ion mode, with Table 2 presenting the relevant data for each compound.

3.2. Mass spectrometric cleavage pathway analysis of the main chemical components of QGC

3.2.1. Flavonoid cleavage pathway

3.2.1.1. Cleavage pathway of Rutin. Rutin ($C_{27}H_{30}O_{14}$, t_R = 4.091 min) displayed a quasi-ion peak $[M - H]^-$ at 609.1469. During secondary mass spectrometric fragmentation, a distinct ion peak at *m/z* 300.02783 was identified. This ion peak is generated when Rutin undergoes loss of its rhamnose and brassinose groups (Fig. 3 A-1).

Table 1
Pathological grading criteria of synovium.

Score	Inflammatory cell infiltration	Synovial hyperplasia	Fibrosis	Macrophage hyperplasia
0	No inflammatory cells	Nothing	Nothing	Nothing
1	20 inflammatory cells infiltrated (each high-power field), sparse and scattered	Monolayer	Minor hyperplasia	Sparse
2	20~50 inflammatory cells infiltrated (per high-power field), dense	2 layers	Moderate hyperplasia	Dense
3	> 50 inflammatory cell infiltration (per high power field), large amount	3 layers	Massive hyperplasia	Massive hyperplasia

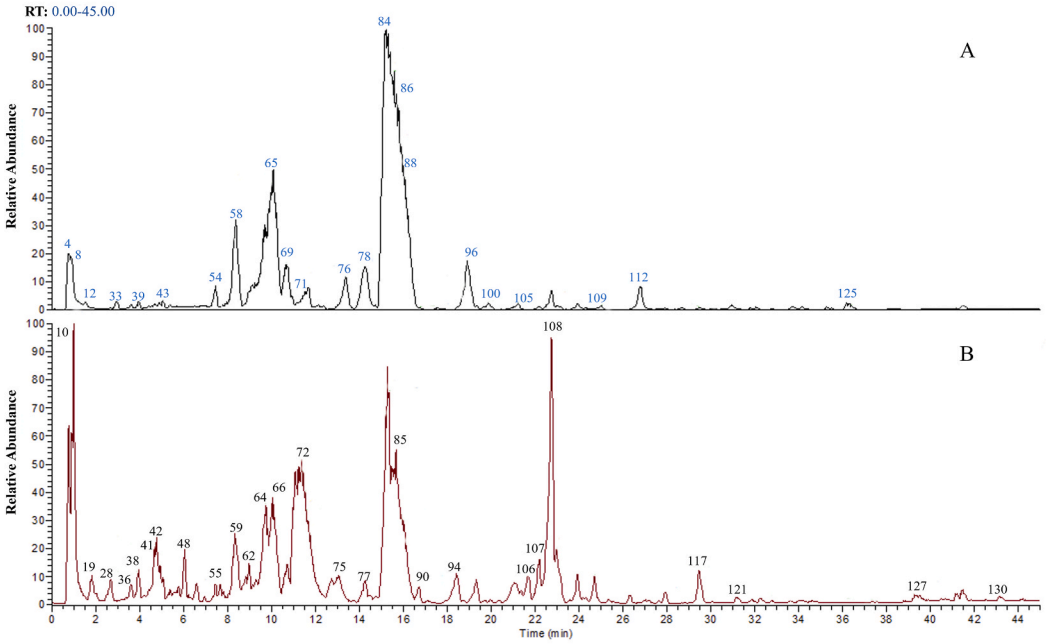

Fig. 2. The total ion flow of QGC. **(A)** Positive ion mode. **(B)** Negative ion mode.

3.2.1.2. Cleavage pathway of Quercetin. The quasi-ionic peak $[M+H]^+$ of Quercetin ($C_{15}H_{10}O_7$, t_R = 8.535 min) was detected at 303.05069. Quercetin was found to undergo cleavage via RDA 0/4 fracture, producing [0,4 A^-] with *m/z* 109.02890. Similarly, RDA 1/3 fracture yielded [1,3 A^-] *m/z* 153.01872, and RDA 1/2 fracture resulted in [1,2 A^-] with *m/z* 180.96608. Subsequent neutral molecule CO loss was followed by further cleavage, generating cleavage ions with *m/z* 153.01872 (Figs. 3 A-2).

3.2.1.3. Cleavage pathway of Astragalin. The quasi-ionic peak $[M-H]^-$ of Astragalin ($C_{21}H_{20}O_{11}$, t_R = 5.566 min) was observed at 447.09384. Upon removal of one molecule of glucose, the fragment ion *m/z* 285.08243 was obtained. Subsequent removal of one H resulted in *m/z* 284.03351, while removal of two H atoms and one molecule of CO first led to the fragment ion *m/z* 255.04077 (Fig. 3 A-3).

3.2.1.4. Cleavage pathway of Rhoifolin. The quasi-ionic peak $[M-H]^-$ of Rhoifolin ($C_{27}H_{30}O_{14}$, t_R = 8.577 min) was measured at 557.15692. Upon removal of one molecule of neohesperulose, the fragment ion *m/z* 269.04575 was obtained, which is the characteristic ion peak of Apigenin (Figs. 3 A-4).

3.2.2. Organic acid cleavage pathway

3.2.2.1. Cleavage pathway of citric acid. Citric acid ($C_6H_8O_7$, t_R = 0.766 min) exhibits a quasi-ionic peak $[M-H]^-$ at 191.01971. When one H_2O is lost, fragment ions are generated at *m/z* 173.00917; the loss of one CO_2 yields fragment ions at *m/z* 129.01939. Additionally, further cleavage by the loss of C_2H_2O results in fragment ions at *m/z* 111.00794 (Figs. 3 B-1).

3.2.2.2. Cleavage pathway of Quinic acid. The quasi-ion peak $[M-H]^-$ of Quinic acid ($C_7H_{12}O_6$, t_R = 1.789 min) was observed at *m/z* 191.05574. Fragment ions were generated in the secondary mass spectrum following the loss of one H_2O (*m/z* 173.04517) and cleaved after the loss of one HCOOH (*m/z* 85.02856) (Figs. 3 B-2).

3.2.3. Coumarins cleavage pathway

3.2.3.1. Cleavage pathway of isoimperatorin. Isoimperatorin ($C_{16}H_{14}O_4$, t_R = 20.090 min) exhibits a quasi-ionic peak $[M+H]^-$ at 293.07815. When the C-5 side chain is lost, a fragment ion with *m/z* 203.03438 is generated, which is followed by the sequential loss of two CO2 molecules leading to the formation of *m/z* 147.04445 (Figs. 3 C-1).

3.2.3.2. Cleavage pathway of osthol. The quasi-ionic peak $[M+H]^+$ for Osthol ($C_{15}H_{16}O_3$, t_R = 19.256 min) was measured at 245.11784. Upon the loss of a C_4H_7 group, fragment ions at *m/z* 189.05519 were observed, followed by further cleavage resulting in

Table 2
Chemical composition information of QGC.

NO.	Component	Formula	t_R/min	Ion	Measured value	ppm	MS^2	Type	Ref.
1	DL-Argine	$C_6H_{14}N_4O_2$	0.668	$[M+H]^+$	175.1195	0.63	70.0660,60.0565	a	[75]
2	4-Guanidinobutyric acid	$C_5H_{11}N_3O_2$	0.723	$[M+H]^+$	146.0926	−0.89	129.0661, 128.0822, 111.0560, 104.0713	c	[76]
3	Choline	$C_5H_{13}NO$	0.734	$[M+H]^+$	104.1076	−0.10	60.0816	n	[77]
4	Betaine	$C_5H_{11}NO_2$	0.74	$[M+H]^+$	118.0868	−0.08	58.0660	f	[77]
5	Maleic acid	$C_4H_4O_4$	0.752	$[M-H]^+$	115.0029	0.00	71.0129	c	[78]
6	DL-Malic acid	$C_4H_6O_5$	0.754	$[M-H]^+$	133.01352	−0.45	115.0029	c	[79]
7	Citric acid	$C_6H_8O_7$	0.766	$[M-H]^+$	191.0197	1.68	173.0092, 129.0194, 111.0079	c	[80]
8	Gluconic acid	$C_6H_{12}O_7$	0.776	$[M-H]^+$	195.0507	−0.26	75.0078	c	[81]
9	Adenine	$C_5H_5N_5$	0.916	$[M+H]^+$	136.0622	0.88	109.0517, 94.0407	b	[82]
10	Adenosine	$C_{10}H_{13}N_5O_4$	0.938	$[M-H]^+$	266.1039	−1.49	134.0622, 117.0357	b	[83]
11	Sucrose	$C_{12}H_{22}O_{11}$	1.144	$[M-H]^+$	341.1093	0.26	71.0129	h	[84]
12	Proline	$C_5H_9NO_2$	1.193	$[M+H]^+$	116.0712	−1.21	70.0660	a	[85]
13	Neochlorogenic acid*	$C_{16}H_{18}O_9$	1.288	$[M-H]^+$	353.0881	−0.99	191.0558	g	[86]
14	Maltol*	$C_6H_6O_3$	1.317	$[M+H]^+$	127.03953	4.60	109.0484, 53.0395	g	[87]
15	2,3-Dihydroxybenzoic acid	$C_7H_6O_4$	1.38	$[M-H]^+$	153.0187	−1.31	125.0240, 109.0287, 96.9591, 69.8197	c	[88]
16	Asperulosidic acid	$C_{18}H_{24}O_{12}$	1.469	$[M-H]^+$	475.2188	−3.58	163.0552	n	[89]
17	D-Fructose	$C_6H_{12}O_6$	1.518	$[M-H]^+$	179.0556	−1.62	114.0237, 89.0235, 71.0129, 59.0129	h	[90]
18	Ephedrine	$C_{10}H_{15}NO$	1.58	$[M+H]^+$	166.1231	−1.26	148.1125, 117.0548	f	[91]
19	D-Quinic acid	$C_7H_{12}O_6$	1.789	$[M-H]^+$	209.0652	−6.08	191.0557, 173.0452, 85.0286	c	[92]
20	Trigonelline	$C_7H_7NO_2$	1.953	$[M+H]^+$	138.0554	−0.22	94.0659, 92.0500	f	[93]
21	2-Lsopropylmalic acid	C7H12O5	2.07	$[M-H]^+$	175.0609	−0.46	113.0600, 73.0285	c	[94]
22	Procyanidin B2	$C_{30}H_{26}O_{12}$	2.216	$[M-H]^+$	577.1370	0.62	425.0884, 407.0777, 289.0721, 125.0237	g	[95]
23	Gentisic acid	$C_7H_6O_4$	2.238	$[M-H]^+$	153.0187	−1.31	108.0208	c	[96]
24	6,7-Dihydroxycoumarin	$C_9H_6O_4$	2.343	$[M-H]^+$	177.0188	−1.64	162.0311	d	[97]
25	Senecionine	$C_{18}H_{25}NO_5$	2.392	$[M+H]^+$	336.1790	−1.99	137.0595	f	[98]
26	Caffeic acid*	$C_9H_8O_4$	2.479	$[M-H]^+$	179.0346	−0.50	135.0444	c	[99]
27	Sinapine	$C_{16}H_{23}NO_5$	2.574	$[M+H]^+$	310.16534	−0.71	292.1546, 251.0920	f	[100]
28	Isophthalic acid	$C_8H_6O_4$	2.61	$[M-H]^+$	165.0187	−1.03	121.0287	c	[101]
29	Benzoic acid	$C_7H_6O_2$	2.617	$[M-H]^+$	121.0287	−0.83	51.3474	c	[102]
30	Catechin*	$C_{15}H_{14}O_6$	2.713	$[M-H]^+$	289.0721	−0.66	245.0821	g	[79]
31	Beta-sitosterol*	$C_{30}H_{52}O$	2.872	$[M+H]^+$	429.7327	−0.93	397.5561, 383.4984、	m	[103]
32	1,3-dimethoxy-2-carboxyanthraquinone	$C_{17}H_{12}O_6$	2.916	$[M-H]^+$	311.0754	−8.04	73.0285	i	[104]
33	Norharman	$C_{11}H_8N_2$	3.06	$[M+H]^+$	169.0764	−0.83	115.0547	n	[105]
34	Cyclo (Leucylprolyl)	$C_{11}H_{18}N_2O_2$	3.318	$[M+H]^+$	211.1449	1.52	86.0972, 70.0660	a	[106]
35	Vanillin	$C_8H_8O_3$	3.644	$[M+H]^+$	153.0555	3.40	125.0602, 111.0447, 83.0498, 65.0394, 55.0188	c	[107]
36	Paracetamol	$C_8H_9NO_2$	3.694	$[M+H]^+$	152.0710	−0.20	109.0528	g	[108]
37	3-Coumaric acid	$C_9H_8O_3$	3.787	$[M-H]^+$	163.0395	−0.12	119.0494	c	[109]
38	4-Coumaric acid	$C_9H_8O_3$	3.79	$[M+H]^+$	165.0551	0.19	119.0497	c	[110]
39	Rutin	$C_{27}H_{30}O_{14}$	4.091	$[M-H]^+$	609.1469	−0.30	463.0780, 300.0278	e	[111]
40	Scopoletin	$C_{10}H_8O_4$	4.249	$[M+H]^+$	193.0500	−1.14	178.0265, 165.0315, 133.0288	f	[112]
41	Quercetin-3β-D-glucoside	$C_{21}H_{20}O_{12}$	4.506	$[M+H]^+$	465.1067	5.53	303.0505, 274.0476	e	[113]
42	2-Hydroxycinnamic acid	$C_9H_8O_3$	4.53	$[M+H]^+$	165.0550	−0.85	147.0444, 123.0809, 91.0549	c	[114]
43	Ferulic acid*	$C_{10}H_{10}O_4$	5.121	$[M-H]^+$	193.0503	−0.73	178.0276, 134.0365	c	[115]
44	Quercetin-3-*O*-pentoside	$C_{20}H_{18}O_{11}$	5.313	$[M-H]^+$	433.0778	−1.75	301.0357, 255.0300, 227.0353, 151.0030	e	[116]
45	Tetrapanoside B	$C_{31}H_{41}NO_7$	5.349	$[M-H]^+$	538.1308	−0.74	358.0669	m	[117]
46	Astragalin	$C_{21}H_{20}O_{11}$	5.566	$[M-H]^+$	447.0938	0.09	285.0824, 284.0335, 255.0408	e	[118]
47	Avicularin	$C_{20}H_{18}O_{11}$	5.77	$[M-H]^+$	433.0779	−0.79	301.0357, 255.0301	b	[119]
48	Daucostero	$C_{35}H_{60}O_6$	6.161	$[M-H]^+$	575.2084	−2.61	413.1559, 177.0502	m	[120]
49	Salicylic acid*	$C_7H_6O_3$	6.465	$[M-H]^+$	137.0237	−0.88	93.0337, 65.0386	c	[121]
50	Neohesperidin	$C_{28}H_{34}O_{15}$	6.72	$[M-H]^+$	609.1821	−3.00	301.0720, 257.0824, 151.0031, 107.0132	e	[122]
51	4,5-Dicaffeoylquinc acid	$C_{25}H_{24}O_{12}$	6.824	$[M-H]^+$	515.1207	0.49	353.0882, 173.0451, 135.0442	c	[123]
52	Rotundine	$C_{21}H_{25}NO_4$	6.977	$[M+H]^+$	356.1864	−0.08	192.1024	n	[124]

(*continued on next page*)

Table 2 (*continued*)

NO.	Component	Formula	t_R/min	Ion	Measured value	ppm	MS^2	Type	Ref.
53	Isorhapontigenin	$C_{15}H_{14}O_4$	7.309	$[M+H]^+$	257.0822	−0.51	241.0500	g	[125]
54	Phloridzin	$C_{21}H_{24}O_{10}$	7.334	$[M-H]^+$	435.2061	1.93	273.0772, 167.0345	e	[126]
55	Luteolin*	$C_{15}H_{10}O_6$	7.62	$[M-H]^+$	285.0408	−0.21	119.1325	e	[127]
56	Dihydrosanguinarine	$C_{20}H_{15}NO_4$	7.96	$[M+H]^+$	334.1080	−0.36	319.0847, 276.0663	n	[128]
57	Baicalin*	$C_{21}H_{18}O_{11}$	8.09	$[M+H]^+$	271.0606	2.26	253.0501, 225.0550	e	[129]
58	Palmatine	$C_{21}H_{21}NO_4$	8.36	$[M+H]^+$	352.1551	0.51	336.1238, 322.1079, 308.1288, 294.1132	c	[130]
59	Berberine*	$C_{20}H_{17}NO_4$	8.526	$[M+H]^+$	336.1240	−0.12	321.0713, 320.0927, 316.1029, 277.0741, 249.0852	f	[131]
60	Quercetin*	$C_{15}H_{10}O_7$	8.535	$[M+H]^+$	303.0507	0.49	180.9661, 153.0187, 109.0289	e	[132]
61	Rhoifolin	$C_{27}H_{30}O_{14}$	8.577	$[M-H]^+$	557.1569	0.90	269.0458	e	[133]
62	Emodin	$C_{15}H_{10}O_5$	8.795	$[M+H]^+$	271.0607	0.11	197.0602, 140.0702	n	[134]
63	Apigetrin*	$C_{21}H_{20}O_{10}$	9.317	$[M-H]^+$	269.0986	−1.15	150.3113, 116.6475	e	[135]
64	Aflatoxin G2	$C_{17}H_{14}O_7$	9.896	$[M+H]^+$	331.0818	−3.78	245.0443	n	[136]
65	Daidzein	$C_{15}H_{10}O_4$	10.012	$[M+H]^+$	255.0657	0.71	93.0496	e	[137]
66	Skimmianin	$C_{14}H_{13}NO_4$	10.273	$[M+H]^+$	260.0908	−3.46	245.0688, 227.0571, 199.0643, 184.0400, 156.0439		[138]
67	Tectoridin	$C_{22}H_{22}O_{11}$	10.341	$[M-H]^+$	461.1095	−0.91	299.0564, 284.0329, 255.0300	e	[139]
68	Diosmetin	$C_{16}H_{12}O_6$	10.373	$[M+H]^+$	301.0713	−0.10	286.0477, 153.0186	e	[140]
69	Kaempferol*	$C_{15}H_{10}O_6$	10.847	$[M+H]^+$	287.0556	−0.45	187.0394	e	[141]
70	Isorhamnetin*	$C_{16}H_{12}O_7$	11.009	$[M+H]^+$	317.0665	−0.57	302.0430, 153.0187	e	[142]
71	Isophorone	$C_9H_{14}O$	11.50	$[M+H]^+$	139.1121	0.50	83.0499, 55.0551	n	[143]
72	Pallasone	$C_{24}H_{38}O_3$	11.575	$[M+H]^+$	375.1605	0.27	189.0344	j	[144]
73	Alizarin-2-methylether	$C_{15}H_{10}O_4$	12.22	$[M+H]^+$	255.2558	−1.57	161.0653	n	[145]
74	Batatasin III	$C_{15}H_{16}O_3$	12.64	$[M-H]^+$	243.1028	−0.82	227.0713	f	[146]
75	Alizarin	$C_{14}H_8O_4$	13.079	$[M-H]^+$	239.0350	−0.54	211.0399, 195.0447, 167.0496, 155.0497	i	[145]
76	Isolariciresinol	$C_{20}H_{24}O_6$	13.389	$[M-H]^+$	359.0779	−0.84	344.0542, 329.0307	n	[121]
77	Camphor	$C_{10}H_{16}O$	13.474	$[M+H]^+$	151.1278	0.07	95.0863	n	[147]
78	Carvone	$C_{10}H_{14}O$	14.365	$[M+H]^+$	151.1121	−1.32	109.0654, 81.0706, 69.0343	k	[148]
79	Nalbuphine	$C_{21}H_{27}NO_4$	14.369	$[M+H]^+$	358.2020	−0.28	217.0866, 167.7816	n	[149]
80	Wogonin	$C_{16}H_{12}O_5$	14.567	$[M+H]^+$	285.0765	−0.84	270.0530	n	[150]
81	Kokusaginine	$C_{14}H_{13}NO_4$	14.594	$[M+H]^+$	258.2570	−3.48	242.2149	n	[151]
82	methyl 6-hydroxy-2,2-dimethyl-3,4-dihydrobenzo[h]chromene-5-carboxylate	$C_{17}H_{18}O_4$	14.596	$[M+H]^+$	259.1132	−0.77	229.0662	n	[133]
83	Nobiletin	$C_{21}H_{22}O_8$	14.80	$[M+H]^+$	403.1397	−1.44	388.1159, 373.0926, 327.0873, 301.0714, 183.0294, 91.0543, 69.0340	n	[152]
84	Genistein	$C_{15}H_{10}O_5$	15.019	$[M-H]^+$	269.04575	0.48	91.3376	e	[153]
85	Glycitein	$C_{16}H_{12}O_5$	15.650	$[M-H]^+$	283.0615	−0.99	268.0379	a	[154]
86	Senkyunolide A	$C_{12}H_{16}O_2$	16.023	$[M+H]^+$	193.1229	0.26	107.0862	n	[155]
87	Lusianthridin	$C_{15}H_{14}O_3$	16.061	$[M-H]^+$	241.0870	−0.50	226.0635, 198.0684, 182.0734	n	[156]
88	Acetophenone	C_8H_8O	16.19	$[M+H]^+$	121.0653	−0.66	103.0549, 93.0706	n	[157]
89	Tangeritin*	$C_{20}H_{20}O_7$	16.523	$[M+H]^+$	373.1292	−1.23	343.0921	e	[158]
90	Demethoxycurcumin	$C_{20}H_{18}O_5$	16.87	$[M+H]^+$	339.1233	−2.89	229.0871, 219.0655, 177.0552, 175.0757	g	[159]
91	Curcumin	$C_{21}H_{20}O_6$	17.151	$[M+H]^+$	369.1339	−2.49	219.0656, 151.0758	g	[160]
92	Mollugin*	$C_{17}H_{16}O_4$	17.910	$[M+H]^+$	285.0984	0.00	60.6673	j	[161]
93	12(13)-DIHOME	$C_{18}H_{34}O_4$	18.03	$[M-H]^+$	313.2387	−1.66	183.1386	n	[162]
94	Rubiadin	$C_{15}H_{10}O_4$	18.412	$[M-H]^+$	253.0507	−0.32	195.0614	i	[163]
95	Sedanolide	$C_{12}H_{18}O_2$	18.424	$[M+H]^+$	195.1385	−0.77	149.1330	n	[164]
96	Ligustilide	$C_{12}H_{14}O_2$	18.595	$[M+H]^+$	191.1072	0.42	173.0966	e	[165]
97	Osthol	$C_{15}H_{16}O_3$	19.256	$[M+H]^+$	245.1178	−0.82	189.0552, 161.0661, 159.0451, 131.0496	d	[166]
98	Xyloidone	$C_{15}H_{12}O_3$	19.382	$[M+H]^+$	241.0865	−0.41	228.0810	j	[167]
99	Nordamnacanthal	$C_{15}H_8O_5$	19.574	$[M+H]^+$	269.0816	−0.74	195.0810	n	[168]
100	4-hydroxy-9,10-dioxoanthracene-2-carboxylic acid	$C_{15}H_8O_5$	19.832	$[M-H]^+$	265.1492	−0.38	96.8592	c	[169]
101	Isoimperatorin	$C_{16}H_{14}O_4$	20.090	$[M+H]^+$	271.0971	−1.22	203.0344, 147.0445	d	[170]
102	Dodecyl sulfate	$C_{12}H_{26}O_4S$	20.094	$[M-H]^+$	265.1481	−0.57	96.9592, 55.4672	n	[171]
103	Nootkatone	$C_{15}H_{22}O$	20.301	$[M+H]^+$	219.1750	−0.78	163.1122, 111.0811	k	[172]
104	Hexadecanedioic acid	$C_{16}H_{30}O_4$	20.870	$[M-H]^+$	285.2073	−0.74	223.2066	c	[104]

(*continued on next page*)

Table 2 (*continued*)

NO.	Component	Formula	t_R/min	Ion	Measured value	ppm	MS^2	Type	Ref.
105	Cryptotanshinone	$C_{19}H_{20}O_3$	21.633	$[M+H]^+$	297.1493	−1.45	254.0945, 221.0967	j	[173]
106	Magnolol	$C_{18}H_{18}O_2$	21.671	$[M-H]^+$	265.1237	−0.23	247.1130	g	[174]
107	7-hydroxy-8-methyl-4-vinyl-9,10-dihydrophenanthrene-1-carboxylic acid	$C_{18}H_{16}O_3$	23.010	$[M+H]^+$	279.3251	8.59	81.0763, 67.0505	c	[169]
108	Abietic acid	$C_{20}H_{30}O_2$	23.064	$[M+H]^+$	303.2326	−0.30	257.2271, 201.1644, 109.1018	c	[175]
109	Levistilide A	$C_{24}H_{28}O_4$	25.382	$[M+H]^+$	381.2055	−5.51	191.1072	i	[176]
110	2′-hydroxymollugin	$C_{17}H_{16}O_4$	25.549	$[M-H]^+$	283.2332	−0.35	86.7286	i	[177]
111	9-hydroxy-octadecadienoic acid	$C_{18}H_{32}O_3$	26.360	$[M-H]^+$	295.2281	−0.61	171.1026	n	[178]
112	Linoleoyl ehanolamide	$C_{20}H_{37}NO_2$	26.658	$[M+H]^+$	324.2905	0.59	306.2802, 109.1017, 95.0962, 62.0609	l	[179]
113	Arachidonic acid	$C_{20}H_{32}O_2$	27.609	$[M+H]^+$	305.2481	−0.69	259.2060	c	[180]
114	Acety-11-keto-β-boswellic acid	$C_{32}H_{48}O_5$	27.701	$[M+H]^+$	513.3590	−0.12	283.2267	c	[181]
115	18-β-Glycyrrhetinic acid	$C_{30}H_{46}O_4$	27.710	$[M+H]^+$	471.3482	−0.13	407.3318, 233.1903, 107.0862	c	[182]
116	Palmitoyl ethanolamide	$C_{18}H_{37}NO_2$	28.395	$[M+H]^+$	300.2905	−0.60	283.2640	l	[183]
117	Oleoyl ethanolamide	$C_{20}H_{39}NO_2$	29.429	$[M+H]^+$	326.3062	−0.18	62.0609	n	[184]
118	Pachymic acid	$C_{33}H_{52}O_5$	29.531	$[M-H]^+$	527.3756	0.93	465.3388	k	[185]
119	Bufalin	$C_{24}H_{34}O_4$	29.599	$[M+H]^+$	387.2513	−0.88	255.3196	n	[186]
120	Hexadecanamide	$C_{16}H_{33}NO$	30.050	$[M+H]^+$	256.2641	−0.47	88.0765	l	[187]
121	Testosterone decanoate	$C_{29}H_{46}O_3$	30.653	$[M+H]^+$	292.3533	0.10	97.1018	n	[188]
122	Lupenone	$C_{30}H_{48}O$	33.084	$[M+H]^+$	425.3817	6.79	217.1958	k	[189]
123	Rubiprasin B	$C_{32}H_{52}O_4$	34.169	$[M-H]^+$	499.3641	0.00	100.3649	k	[190]
124	Stearamide	$C_{18}H_{37}NO$	34.230	$[M+H]^+$	284.2954	0.00	130.1230, 116.1075, 102.0919, 88.0764, 74.0608, 57.0707	l	[191]
125	Sitosterol	$C_{29}H_{50}O$	36.892	$[M\text{-}H2O+H]^+$	397.7630	−1.51	107.0532, 55.8619	m	[192]
126	Bis(2-ethylhexyl)adipate	$C_{22}H_{42}O_4$	38.039	$[M+H]^+$	371.3190	7.62	147.0655	n	[193]
127	Ginkgolic acid (C17:1)	$C_{24}H_{38}O_3$	39.051	$[M-H]^+$	373.2752	−0.56	329.2853	c	[194]
128	Ethyl oleate	$C_{20}H_{38}O_2$	40.647	$[M+H]^+$	311.2948	−1.28	265.2539, 247.2428	c	[195]
129	Paryriogenin I	$C_{26}H_{31}O_2$	42.982	$[M+H]^+$	423.3740	−0.74	111.0706	m	[196]
130	Ergocalciferol	$C_{28}H_{44}O$	43.864	$[M+H]^+$	397.3471	−0.08	81.0707, 69.0707	m	[197]

Note: a. Amino acids; **b.** Nucleosides and their bases; **c.** Organic acids; **d.** Coumarins; **e.** Flavonoids; **f.** Alkaloids; **g.** Polyphenols; **h.** Sugars; **i.** Anthraquinones; **j.** Quinones; **k.** Terpenoids; **l.** Amides; **m.** Sterols; **n.** Others. *For comparison using controls.

fragment ions at *m/z* 161.06612 $[M + H–C4H7–CO]^+$, *m/z* 159.04507 $[M + H–C4H7–CH2O]^+$, and *m/z* 131.04964 $[M + H–C4H7–CO–CH2O]^+$ (Figs. 3 C-2).

3.2.3.3. Cleavage pathway of scopoletin lactone. The quasi-ionic peak $[M+H]^+$ of Scopoletin ($C_{10}H_8O_4$, t_R = 4.249 min) was observed at 193.05000. A fragment ion with *m/z* 178.02654 is formed when methoxy is lost from the benzene ring. Furthermore, the loss of one molecule of CO at the lactone position results in a fragment with *m/z* 165.03149. Subsequently, the loss of CH^{3+} from the methoxy on the benzene ring, along with the removal of the neighboring OH on the benzene ring, leads to the formation of a fragment ion with *m/z* 133.02881 (Fig. 3 C-3).

3.2.4. Polyphenols cleavage pathway

3.2.4.1. Cleavage pathway of neochlorogenic acid. Neochlorogenic acid ($C_{16}H_{18}O_9$, t_R = 1.288 min) exhibits a quasi-ionic peak $[M-H]^-$ at 353.08847. Upon the loss of one caffeoyl molecule (-$C_9H_6O_3$), a distinct fragment ion *m/z* 191.05577 is generated. Subsequently, the further loss of one molecule of H_2O results in the production of *m/z* 173.04508 (Figs. 3 D-1).

3.2.4.2. Cleavage pathway of Procyanidin B2. The quasi-ionic peak $[M-H]^-$ of Procyanidin B2 ($C_{30}H_{26}O_{12}$, t_R = 2.216 min) was observed at 577.13696. Upon deletion of $C_8H_8O_3$, the molecule underwent RDA cleavage and rearrangement resulting in the fragment ion *m/z* 425.08835. Further removal of one molecule of H_2O led to the formation of *m/z* 407.07773. Alternatively, two catechins were broken down to yield fragment ions *m/z* 289.07214, with the deletion of $C_9H_8O_3$ and rearrangement producing fragment ions *m/z* 125.02366 (Figs. 3 D-2).

3.2.4.3. Cleavage pathway of catechin. Catechin ($C_{15}H_{14}O_6$, t_R = 2.713 min) exhibits a quasi-ionic peak $[M-H]^-$ at 289.07208. Upon removal of one molecule of CO2, fragment ions at *m/z* 245.08212 are observed. Subsequent loss of another molecule of C_2H_2O and rearrangement results in fragment ions at *m/z* 203.05282, followed by further loss of one molecule of C_2H_2O leading to fragment ions at *m/z* 161.05002 (Fig. 3 D-3).

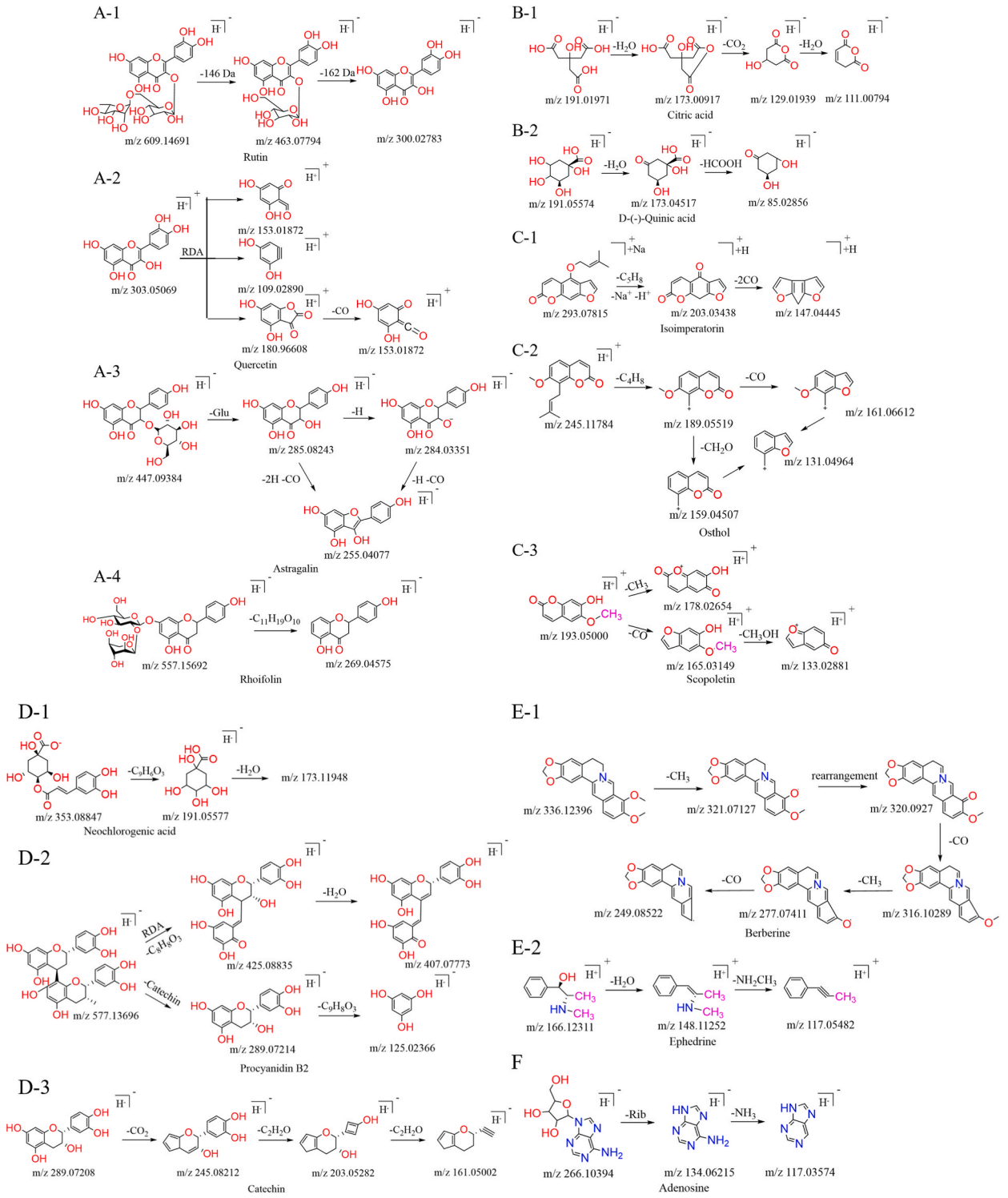

Fig. 3. Diagram of the major fragment cleavage pathways for the chemical composition of QGC. **(A)** Flavonoids. **(B)** Organic acids. **(C)** Coumarins. **(D)** Polyphenols. **(E)** Alkaloids. **(F)** Nucleosides.

3.2.5. Alkaloids cleavage pathway

3.2.5.1. Cleavage pathway of berberine. The quasi-ionic peak $[M+H]^+$ of Berberine ($C_{20}H_{17}NO_4$, t_R = 8.526 min) was measured at 336.12396. A characteristic fragment ion at *m/z* 321.07127 is generated through the loss of a methyl group, followed by *m/z* 320.0927 after rearrangement and the loss of an H, and finally *m/z* 249.08522 (Figs. 3 E−1).

3.2.5.2. Cleavage pathway of Ephedrine. Ephedrine ($C_{10}H_{15}NO$, t_R = 1.58 min) exhibits a quasi-ionic peak $[M+H]^+$ at 166.12311. Subsequent fragmentation resulted in the formation of a fragment ion at *m/z* 148.11252 following the loss of one molecule of H_2O, and further removal of $–NH_2$-CH_3 yielded a fragment at *m/z* 117.05482 (Figs. 3 E−2).

3.2.6. Nucleosides cleavage pathway

3.2.6.1. Cleavage pathway of Adenosine. The quasi-ionic peak $[M - H]^-$ of Adenosine ($C_{10}H_{13}N_5O_4$, t_R = 0.938 min) was observed at 266.10394. Subsequently, a fragment ion of *m/z* 134.06215 was obtained after the loss of one ribose molecule, followed by the loss of NH3 resulting in a fragment ion of *m/z* 117.03574 (Fig. 3 F).

3.3. Drug active ingredient screening and target collection

A total of 130 compounds were identified through liquid mass analysis. Among these, 44 compounds were identified as potentially active based on their ADME properties using TCMSP and Uniprot databases. The screening criteria required OB to be equal to or greater than 30 % and DL to be equal to or greater than 0.18. After eliminating duplicate compounds, there remained 39 potentially active compounds, representing 30.00 % of the initial 130 compounds. Furthermore, the removal of duplicate targets resulted in a total of 234 targets associated with the drug components. The basic information of the active ingredients can be found in Table 3.

Table 3
List of active compounds in accordance with screening criteria OB and DL.

MOL ID	MOL name	OB%	DL	CAS
MOL001463	Dihydrosanguinarine	59.31	0.86	3606-45-9
MOL001454	Berberine	36.86	0.78	633-66-9
MOL002776	Baicalin	40.12	0.75	31564-28-0
MOL000785	Palmatine	64.6	0.65	3486-67-7
MOL005828	Nobiletin	61.67	0.52	478-01-3
MOL007088	Cryptotanshinone	52.34	0.40	35825-57-1
MOL006407	Neochlorogenic acid	18.05	0.33	906-33-2
MOL000354	Isorhamnetin	49.60	0.31	480-19-3
MOL000098	Quercetin	46.43	0.28	73123-10-1
MOL001798	Neohesperidin	71.17	0.27	13241-33-3
MOL002881	Diosmetin	31.14	0.27	520-34-3
MOL000006	Luteolin	36.16	0.25	491-70-3
MOL000492	Catechin	54.83	0.24	154-23-4
MOL000422	Kaempferol	41.88	0.24	520-18-3
MOL008400	Glycitein	50.48	0.24	40957-83-3
MOL000173	Wogonin	30.68	0.23	632-85-9
MOL001942	Isoimperatorin	45.46	0.23	482-45-1
MOL005320	Arachidonic acid	45.57	0.20	7771-44-0
MOL008599	Ethyl oleate	32.40	0.19	111-62-6
MOL004071	Rotundine	73.94	0.64	483-14-7
MOL013271	Kokusaginine	66.68	0.20	484-08-2
MOL002663	Skimmianin	40.14	0.20	83-95-4
MOL000358	β-sitosterol	36.91	0.75	83-46-5
MOL003283	Isolariciresinol	66.51	0.39	548-29-8
MOL000359	Sitosterol	36.91	0.75	83-46-5
MOL005638	Mollugin	42.34	0.26	55481-88-4
MOL005869	Daucostero_qt	36.91	0.75	474-58-8
MOL006139	1,3-dimethoxy-2-carboxyanthraquinone	102.89	0.33	–
MOL006153	2′-hydroxymollugin	40.50	0.29	154706-45-3
MOL006147	Alizarin-2-methylether	32.81	0.21	6003-11-8
MOL006149	7-hydroxy-8-methyl-4-vinyl-9,10-dihydrophenanthrene-1-carboxylic acid	56.99	0.27	–
MOL006150	1-acetoxy-6-hydroxy2-methylanthraquinone-3-*O*-α-rhamnosyl (1 → 4)-α-glucoside	30.74	0.64	–
MOL006155	4-hydroxy-9,10-dioxoanthracene-2-carboxylic acid	45.98	0.25	25186-77-0
MOL006162	Nordamnacanthal	53.97	0.24	3736-59-2
MOL006164	Pallasone	43.87	0.40	56495-82-0
MOL006167	methyl 6-hydroxy-2,2-dimethyl-3,4-dihydrobenzo[h]chromene-5-carboxylate	51.09	0.25	–
MOL006174	Xyloidone	31.61	0.18	15297-92-4
MOL008020	Paryriogenin I	45.26	0.79	–
MOL008025	Tetrapanoside B_qt	40.93	0.79	–

3.4. Screening of GA related targets

To identify targets related to GA, a search was conducted in databases such as TTD, Drugbank, and DisGeNET. Uniprot IDs were standardized using the Uniprot database. Targets lacking Uniprot IDs or gene information were excluded, leading to a final list of 206 targets associated with gout disease.

3.5. Intersection of drug active ingredient action genes and GA disease genes

GA-related genes were identified from the disease database, yielding 206 genes that were standardized using the Uniprot database. Through VENNY 2.1 online mapping software, 16 intersecting targets were found by comparing the active ingredient targets of QGC with gout disease-related targets (Table 4, Fig. 4A). These 16 genes are associated with 11 of the 39 active ingredients, including dihydrosanguinarine, nobiletin, isorhamnetin, quercetin, luteolin, kaempferol, glycitein, wogonin, β-sitosterol, isolariciresinol, and xyloidone. A network linking "drug-active ingredient-disease target-GA" was established (Fig. 4B), suggesting that QGC may influence these 16 target protein genes through the mentioned 11 active ingredients, thereby potentially exerting a therapeutic effect on GA.

3.6. PPI network construction results and analysis

The PPI network graph comprises 16 nodes and 54 edges, with an average degree of 6.75. Out of the 16 cross targets, two non-interaction targets were excluded (Fig. 4C). Subsequently, an analysis of the degree values of the remaining 14 targets was conducted. The findings revealed that the top five targets with the highest degree values were PPARG (degree = 24), IL-6 (degree = 24), MMP-9 (degree = 22), IL-1β (degree = 22), and CXCL8 (degree = 20) (Fig. 4D). In summary, these results suggest that these targets play a crucial role in the treatment of GA by QGC.

3.7. GO enrichment analysis

The 16 screened targets were subjected to GO analysis with a significance threshold of $p < 0.05$. The most notable enrichment results were chosen to categorize BP, MF, and CC as illustrated in Fig. 5. The BP analysis yielded 69 entries, predominantly linked to positive regulation of gene expression, inflammatory response, angiogenesis, transcription from RNA polymerase II promoter, transcription by DNA template, and other processes. The MF analysis uncovered 11 entries, primarily associated with protein binding, zinc ion binding, identical protein binding, cytokine activity, integrin binding, and other functions. The CC analysis identified 3 entries, mainly localized in the extracellular space, extracellular region, and perinuclear region of cytoplasmic components.

3.8. KEGG enrichment analysis

The DAVID database was used to import the 16 common targets for KEGG enrichment analysis, resulting in the identification of 47 pathways with $p < 0.05$. The top 15 pathways were selected for further analysis, and KEGG pathway bubble maps were generated using the Microbiology Online Mapping website (Fig. 6A). The enrichment analysis of targets in KEGG indicated involvement of IL-17, rheumatoid arthritis, mitogen-activated protein kinase (MAPK), PI3K/Akt, and other pathways. A graph in Fig. 6B illustrates the enrichment results of the core targets in the IL-17 pathway. These findings suggest that the therapeutic effect of QGC on GA may encompass a complex biochemical process with multiple components, targets, and pathways.

Table 4
Intersection of action genes of active ingredients of QGC and GA disease genes.

NO.	Gene Full Name	Gene	Uniprot ID
1	ATP binding cassette subfamily G member 2 (Junior blood group)	ABCG2	Q9UNQ0
2	Arachidonate 5-lipoxygenase	ALOX5	P09917
3	C-reactive protein	CRP	P02741
4	C-X-C motif chemokine ligand 8	CXCL8	P10145
5	Hepatocyte growth factor	HGF	P14210
6	Interleukin 1 alpha	IL1A	P01583
7	Interleukin 1 beta	IL1B	P01584
8	Interleukin 6	IL6	P05231
9	Insulin receptor	INSR	P06213
10	Matrix metallopeptidase 9	MMP9	P14780
11	Nuclear factor, erythroid 2 like 2	NFE2L2	Q16236
12	Peroxisome proliferator activated receptor delta	PPARD	Q03181
13	Peroxisome proliferator activated receptor gamma	PPARG	P37231
14	Protein kinase C alpha	PRKCA	P17252
15	Glycogen phosphorylase, muscle associated	PYGM	P11217
16	Secreted phosphoprotein 1	SPP1	P10451

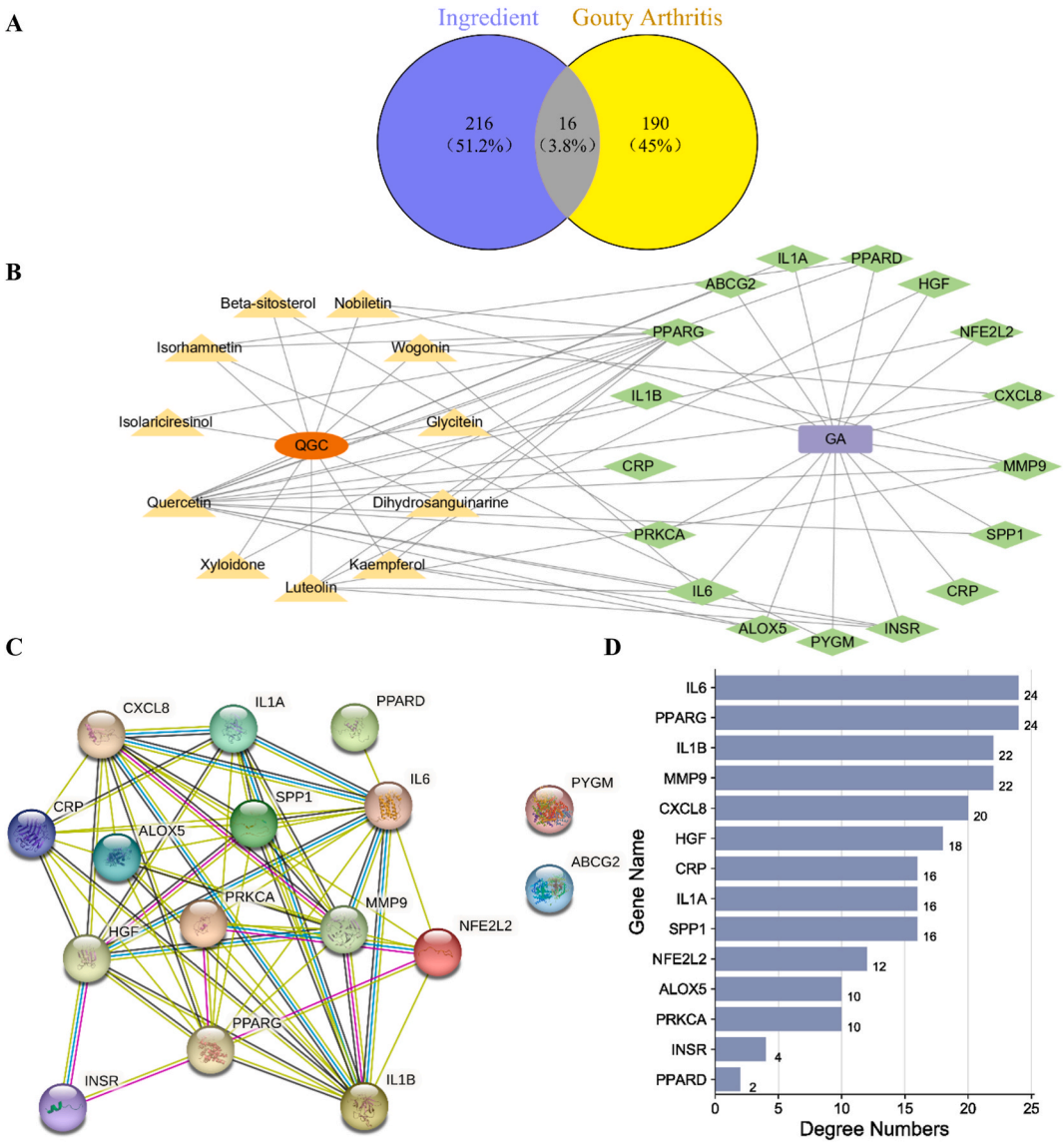

Fig. 4. The active substance-treatment target-PPI-gene expression of QGC. **(A)** Venn diagram of active compound target and disease target. **(B)** Drug active component target protein gene GA network diagram of QGC. In the diagram, the oval stands for the drug QGC, while the triangle represents its active compound and the diamond symbolizes the target gene, and the square represents the GA disease. **(C)** PPI. **(D)** Gene expression profile.

3.9. Molecular docking

The results of PPI and KEGG analyses were used to perform molecular docking with the CB-DOCK2 online platform. The purpose of this docking was to identify potential active compounds (Kaempferol, Luteolin, Nobiletin, Quercetin, and Wogonin) and target proteins (CXCL8, IL-1β, IL-6, MMP9, and PPARG). The results showed that Kaempferol, Luteolin, Nobiletin, Quercetin, and Wogonin had strong binding affinity to the therapeutic targets CXCL8, IL-1β, IL-6, MMP9, and PPARG. These findings are consistent with those from the network pharmacological analysis (Fig. 7A–F).

3.10. Effect of QGC on swelling degree of ankle joint in GA model rats

After establishing a GA model of rat ankle joint, it was found that the ankle joint swelling in the model group was significantly higher compared to the normal group ($p < 0.01$). Interestingly, the high-dose group of QGC showed a significant reduction in ankle joint swelling 24 h after modeling. Similarly, the positive drug colchicine (0.2 mg/kg) group also exhibited a significant decrease in ankle joint swelling at 8 and 24 h post-modeling ($p < 0.05$) (Table 5).

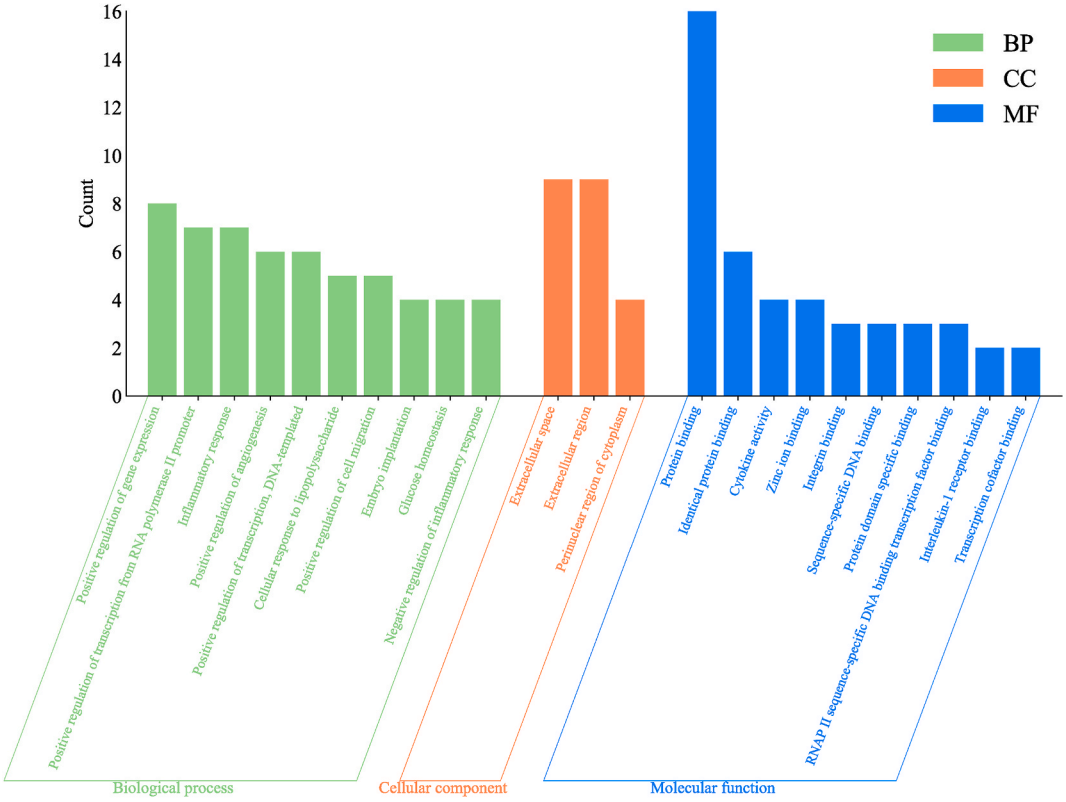

Fig. 5. Go function analysis.

3.11. Effect of QGC on synovial histopathology of ankle joint in GA model rats

Histopathological analysis of synovial tissue in normal rats revealed a typical morphology and structure, characterized by well-organized cells and 1–2 layers of synovial cells on the membrane surface. In contrast, the model group displayed an irregular joint surface with disordered cell arrangement, connective tissue infiltration, and disruption of the synovial tissue structure. All six rats in the model group exhibited increased cell proliferation, varying levels of inflammatory cell infiltration and mononuclear macrophages in the synovial membrane, and fibrous tissue proliferation in five cases. Treatment with colchicine led to a smoother and flatter joint surface, reduced inflammatory cell infiltration in the synovial membrane, decreased proliferation of synovial tissue and fibroblasts, and reduced macrophage proliferation. While low and medium-dose QGC treatment had some effects, the high-dose group showed a smooth and flat joint surface with more organized cell arrangement and clear structure, minimal or no hyperplasia of fibrous and synovial tissues, minimal inflammatory cell infiltrations in the synovial membrane, and no macrophage hyperplasia. Pathological scores analysis revealed a significant increase in synovial membrane pathology score in the model group compared to the normal group ($p < 0.01$). However, treatment with colchicine and high-dose QGC significantly reduced the synovial pathology score ($p < 0.05$), while the low and medium-dose QGC groups did not show substantial changes in synovial pathology score ($p > 0.05$) (Fig. 8A–F).

3.12. ELISA and biochemical assays

Compared to the control group, TNF-α (Fig. 9A), IL-6 (Fig. 9B), and MDA (Fig. 9D) levels were significantly elevated ($p < 0.05$) in the model group, while SOD (Fig. 9C) levels were significantly reduced ($p < 0.001$). However, both the positive drug and QGC administration groups demonstrated a reversal of these changes when compared to the model group (Fig. 9).

3.13. Validation of key pathway-related core targets of QGC for GA treatment

Following network pharmacological screening, we conducted immunohistochemistry analysis to validate key pathway-related targets (Fig. 10A). Our findings showed a significant decrease in levels of CXCL8 (Fig. 10B) and PPARG (Fig. 10F) ($p < 0.001$), while IL-1β (Fig. 10C), IL-6 (Fig. 10D), and MMP9 (Fig. 10E) exhibited a significant increase ($p < 0.01$) in the ankle synovial tissue of the model group compared to the normal group. Subsequently, positive drug administration led to significant increases in CXCL8 and PPARG levels ($p < 0.01$), with a decrease in IL-1β, IL-6, and MMP9 levels ($p < 0.05$) compared to the model group. Specifically, in the high-dose QGC group, CXCL8 levels were significantly elevated ($p < 0.05$), while IL-1β, IL-6, and MMP9 were greatly reduced ($p <$

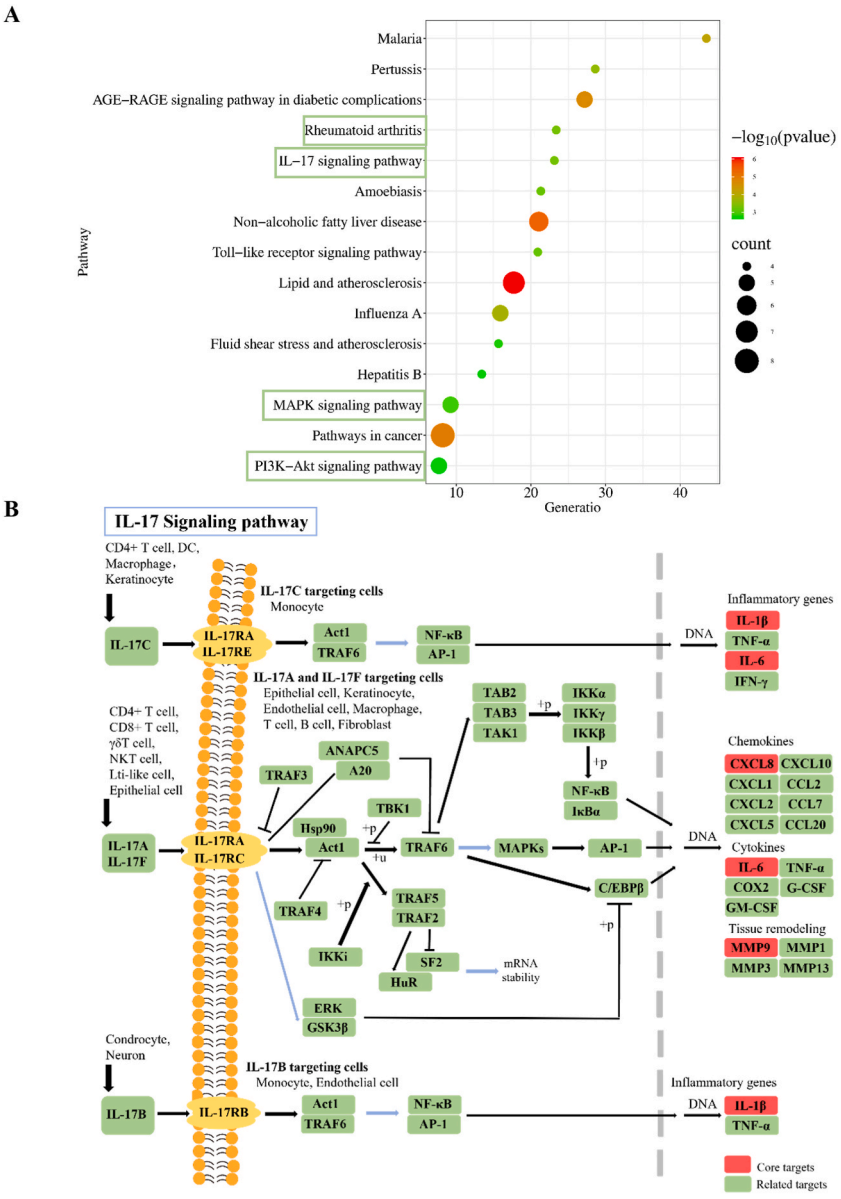

Fig. 6. KEGG analysis. **(A)** Bubble diagram of KEGG pathway treated with GA by QGC. The visual representation of the data includes a horizontal axis that represents the enrichment factor and a vertical axis that represents the pathway. The color of each bubble corresponds to the corrected *p* value, with green indicating a larger value and red indicating a smaller value. As the corrected *p* value decreases, the enrichment becomes more significant. The size of each bubble corresponds to the number of genes enriched in that particular pathway. **(B)** The enrichment results of QGC in IL-17 signal pathway. Green represents relevant targets, arrows represent pathways, red pentagrams indicate enrichment of the screened core targets in the IL-17 signaling pathway.

0.05) compared to the model group, with no significant change observed in PPARG. In the mid-dose group, CXCL8 levels were significantly increased ($p < 0.05$), and IL-1β and MMP9 levels were significantly decreased ($p < 0.01$) compared to the model group, while IL-6 and PPARG showed no significant changes. Finally, in the low-dose group, PPARG levels were significantly increased ($p < 0.01$), and IL-1β and MMP9 levels were markedly decreased ($p < 0.05$) compared to the model group, while CXCL8 and IL-6 showed no significant changes.

4. Discussion

The clinical manifestations of gout involve recurrent episodes of sudden joint pain, hyperuricemia, and MSU crystal deposition [14, 15]. Gout is characterized by the deposition of MSU crystal aggregates in and around joints and soft tissues, leading to bone erosion

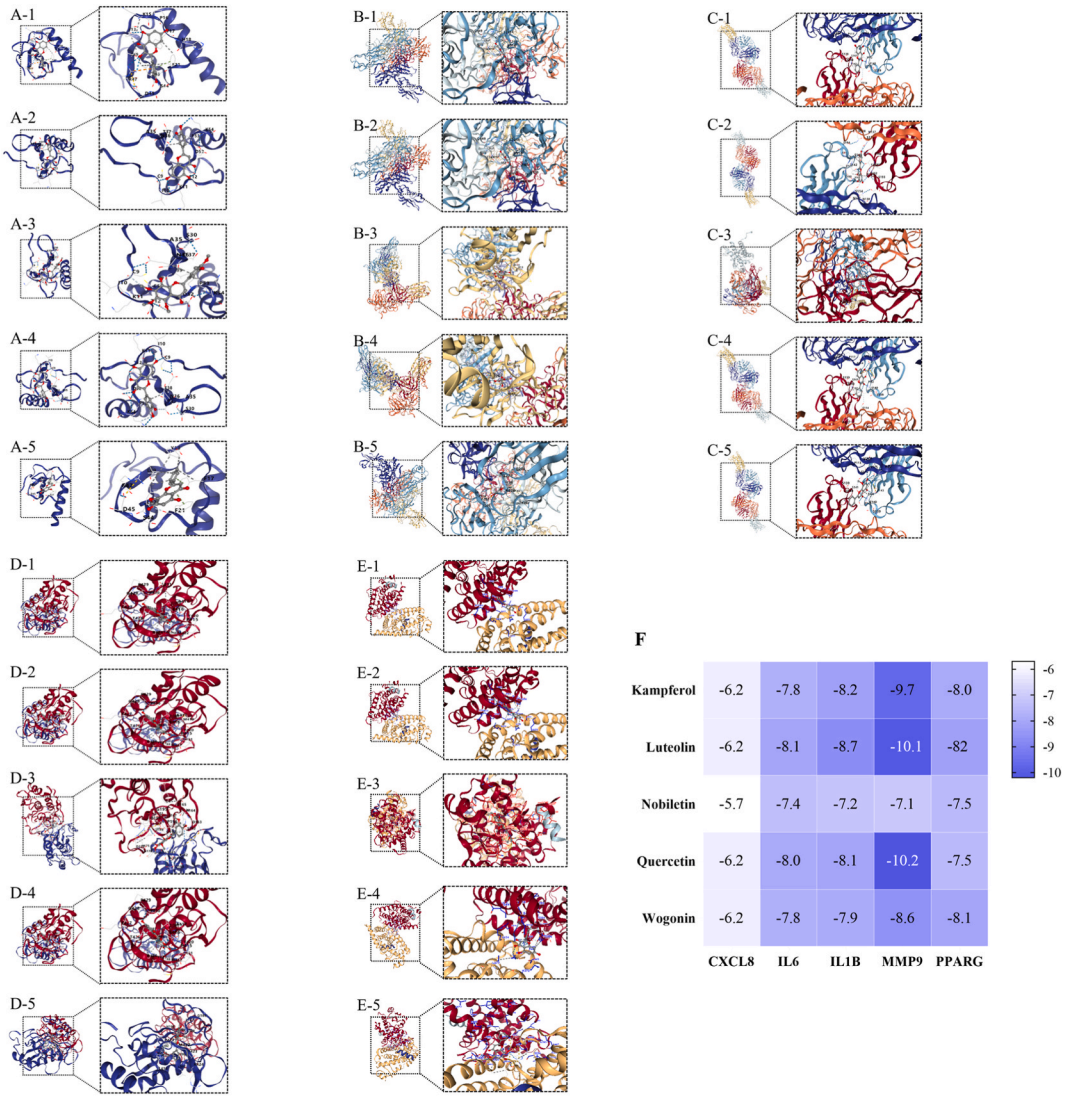

Fig. 7. Molecular docking diagram and cluster heat diagram of QGC. **(A)**, Kaempferol **(B)**, Luteolin **(C)**, Nobiletin **(D)**, Quercetin **(E)**, Wogonin; **1**: Docking with CXCL8 receptor protein; **2**: Docking with IL-6 receptor protein; **3**: Docking with IL-1β receptor protein; **4**: Docking with MMP9 receptor protein; **5**: Docking with PPARG receptor protein **(F)**, Cluster heat diagram of QGC.

Table 5
Comparison of ankle joint swelling in rats of different treatment groups.

Group	Number	Dose (mg/kg)	Ankle joint swelling/(%)				
			1 h	3 h	5 h	8 h	24 h
Normal	6	–	1.08 ± 0.59	4.19 ± 1.58	9.45 ± 4.66	4.52 ± 1.26	2.84 ± 0.62
Model	6	–	10.78 ± 2.28	38.49 ± 3.60	34.78 ± 3.07	40.26 ± 3.28	36.12 ± 2.85
Colchicine	6	0.2	11.09 ± 2.08	33.31 ± 2.17	28.89 ± 2.39	27.73 ± 2.56*	16.64 ± 1.60*
Low	6	95	10.17 ± 1.30	33.40 ± 2.69	32.69 ± 2.95	36.56 ± 2.57	31.96 ± 2.20
Medium	6	190	9.73 ± 2.79	34.45 ± 5.69	31.35 ± 4.91	37.01 ± 4.52	32.70 ± 4.21
High	6	378	10.85 ± 1.21	32.18 ± 3.65	29.63 ± 4.65	29.49 ± 3.95*	17.64 ± 3.20*

Note: Compared with the model group, $*p < 0.05$.

[16]. Gout attacks are linked to high levels of uric acid in the body and have a genetic component, more prevalent in men over 40 [17,18]. Classified as a type of metabolic rheumatism, gout is directly associated with hyperuricemia, resulting from abnormalities in purine metabolism or decreased uric acid excretion [19,20]. If left untreated, gout can lead to complications like renal lesions, joint damage, deformities, musculoskeletal disability, and renal function impairment, as well as hyperlipidemia, hypertension, diabetes,

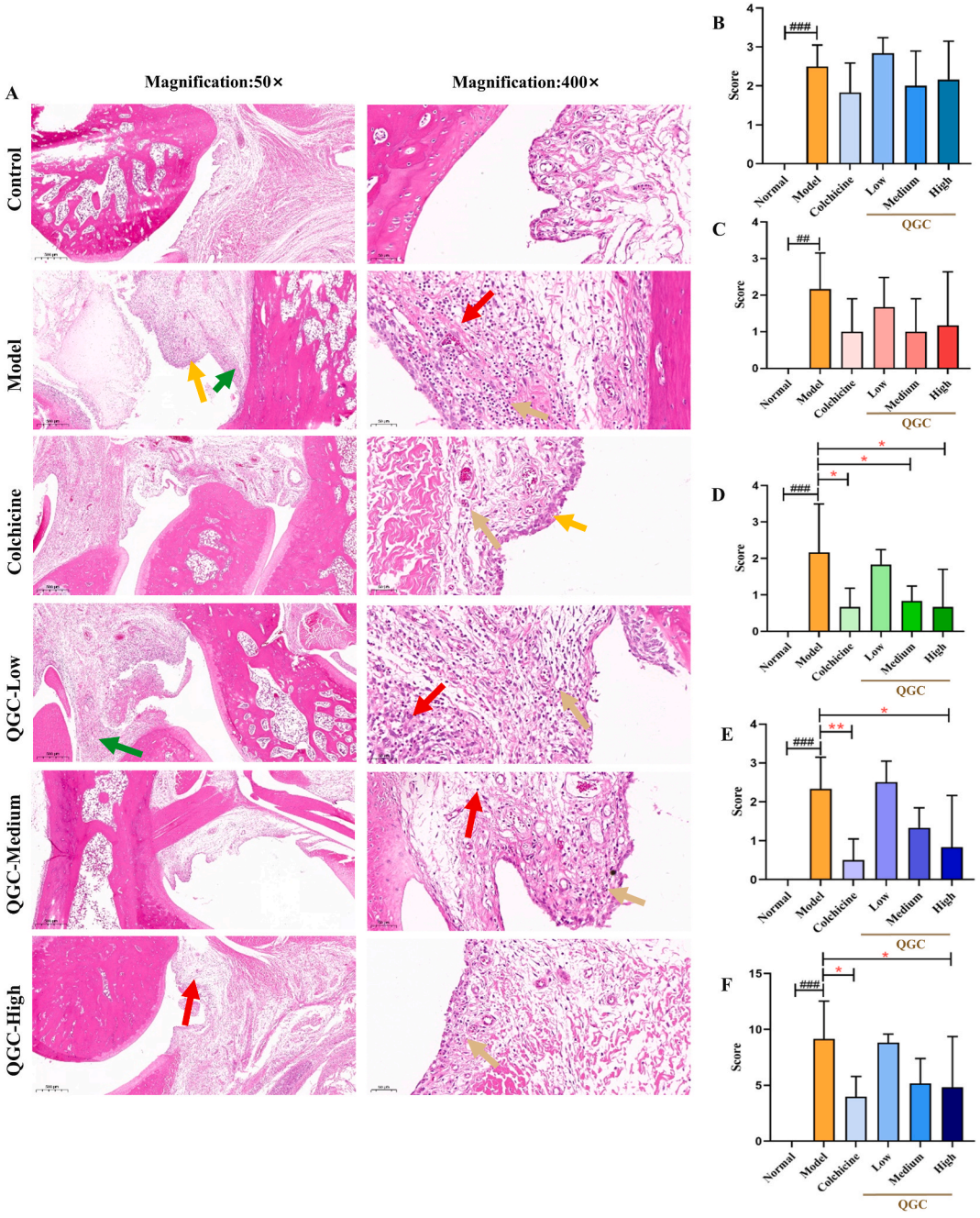

Fig. 8. The histopathological evaluation of synovium of ankle joint of rats in different treatment groups by HE staining (n = 6; magnification: × 50 and × 400; Scales: 500 and 50 μm). **(A)** Brown arrow-inflammatory cell infiltration, red arrow-increased monocyte macrophages, orange arrow synovial tissue hyperplasia with exudation and edema, green arrow-local fibrous tissue hyperplasia. **(B)** Inflammatory cell infiltration score. **(C)** Synovial hyperplasia score. **(D)** Fibrous tissue hyperplasia score. **(E)** Macrophage proliferation score. **(F)** Total score of single samples. Compared with the normal group, $^{\#\#}p < 0.01$, $^{\#\#\#}p < 0.001$. Compared with the model group, $^{*}p < 0.05$, $^{**}P < 0.01$.

atherosclerosis, and coronary artery disease [21–23]. These complications pose significant risks to patients' health and well-being. Chinese medicine, a valuable tradition with exceptional benefits in treating complex diseases like gout, often employs a combination of multiple herbs, following a "multi-components, multi-targets" approach. Therefore, employing a systems pharmacology approach can help identify the active ingredients and pathways of traditional Chinese medicine (TCM), offering valuable insights into understanding TCM mechanisms.

The efficacy of Qinggan Capsule (QGC) on gouty arthritis (GA) remains unknown. Initially, we identified the ingredients in QGC

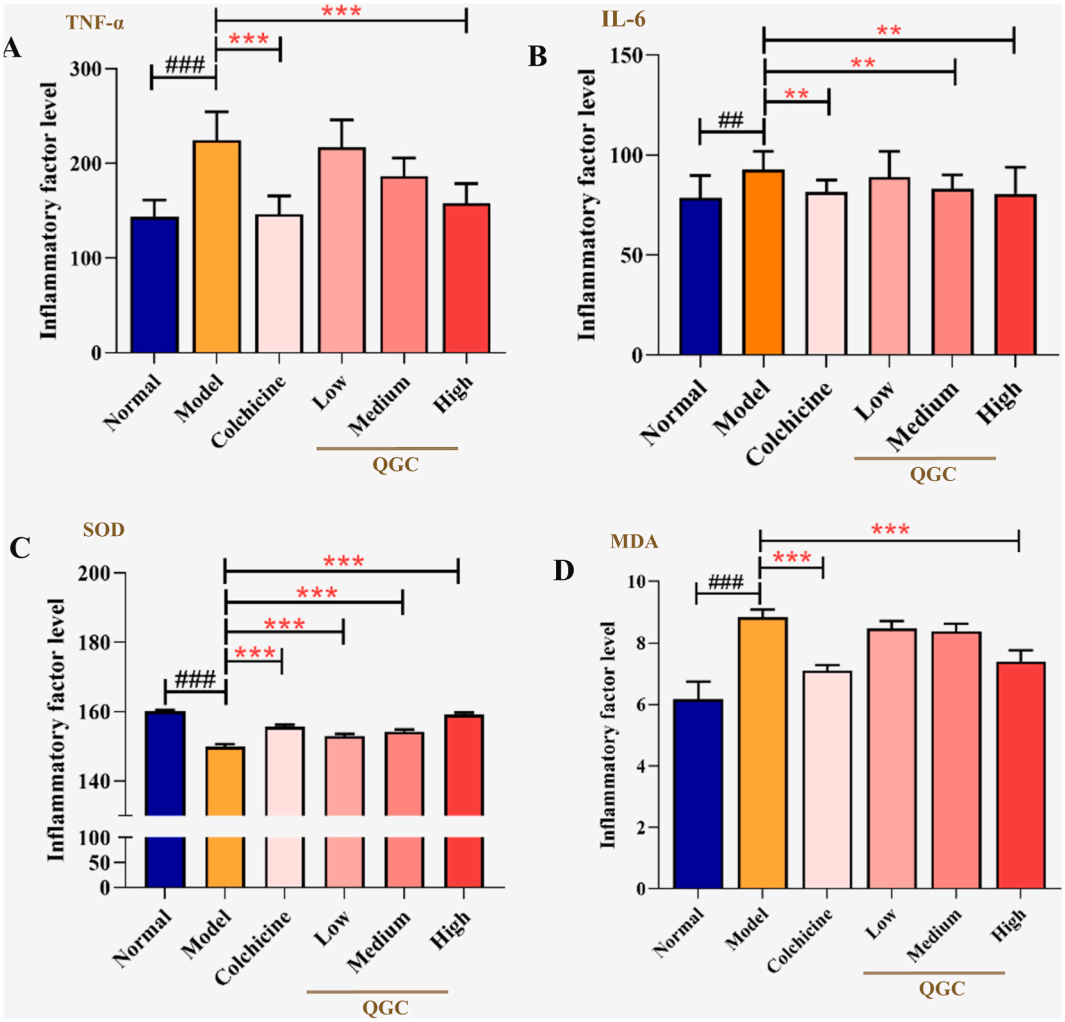

Fig. 9. The expression level of TNF-α **(A)**, IL-6 **(B)**, SOD **(C)** and MDA **(D)** in rats of different treatment groups (n = 6). Compared with the normal group, $^{\#\#}p < 0.01$, $^{\#\#\#}p < 0.001$. Compared with the model group, $^{**}p < 0.01$, $^{***}p < 0.001$.

using the UPLC-Q Exactive-MS technique. Our results indicated that QGC primarily consists of compounds such as coumarins, flavonoids, alkaloids, polyphenols, anthraquinones, quinones, terpenoids, amides, and sterols. Notably, genistein, acetophenone, and tangeritin are among the compounds with higher content. Subsequently, we conducted a comprehensive analysis of the chemical composition of each drug in QGC, identifying 44 potential active components and 234 potential targets across the prescription through meticulous technical analysis. Further scrutiny revealed that 39 chemical components, including berberine, baicalin, palmatine, nobiletin, neochlorogenic acid, quercetin, luteolin, catechin, kaempferol, glycitein, wogonin, rotundine, mollugin, and xyloidone, met the screening criteria and could serve as effective components of drugs. For instance, berberine shows promise in preventing GA and reducing inflammatory responses due to its anti-inflammatory, antibacterial, neuroprotective, and immune-regulating properties [24–27], and can reduce the expression of inflammatory factors such as MMP-9, TNF-α, and IL-6 [28]. Baicalin, sourced from the root of Scutellaria baicalensis, possesses beneficial effects such as anti-viral, anti-bacterial, and anti-oxidative properties [29–31]. Past research [32–34] has illustrated that baicalin can influence the expression of FOXP3 and STAT3, along with regulating downstream cytokines like IL-1β, IL-4, and IL-5 by inhibiting nuclear NF-κB expression. Palmatine, an isoquinoline alkaloid found naturally, has demonstrated preventive effects against Metabolic Syndrome (MetS), cardiovascular disease, osteoporosis, and osteoarthritis, potentially linked to MetS. These protective properties are attributed to its antioxidant and anti-inflammatory characteristics [35]. Nobiletin, a polymethoxyflavonoid, showcases anti-inflammatory, neuroprotective, antioxidant, and antitumor properties [36]. Mollugin, derived from Rubia cordifolia, is a naphthoquinone compound with anti-inflammatory, antitumor, and antiviral attributes, commonly used in treating colitis, arthritis, and uterine inflammation [37–39]. In conclusion, the study provides compelling evidence supporting the importance of these ingredients in the anti-GA effects of QGC. To visually represent the overlap of various factors, a Venn diagram was employed. In the context of drug therapy, precise targeting of specific diseases necessitates binding to particular targets. To achieve this, the VENNY 2.1 online mapping tool was utilized to examine the binding targets of the active ingredients and

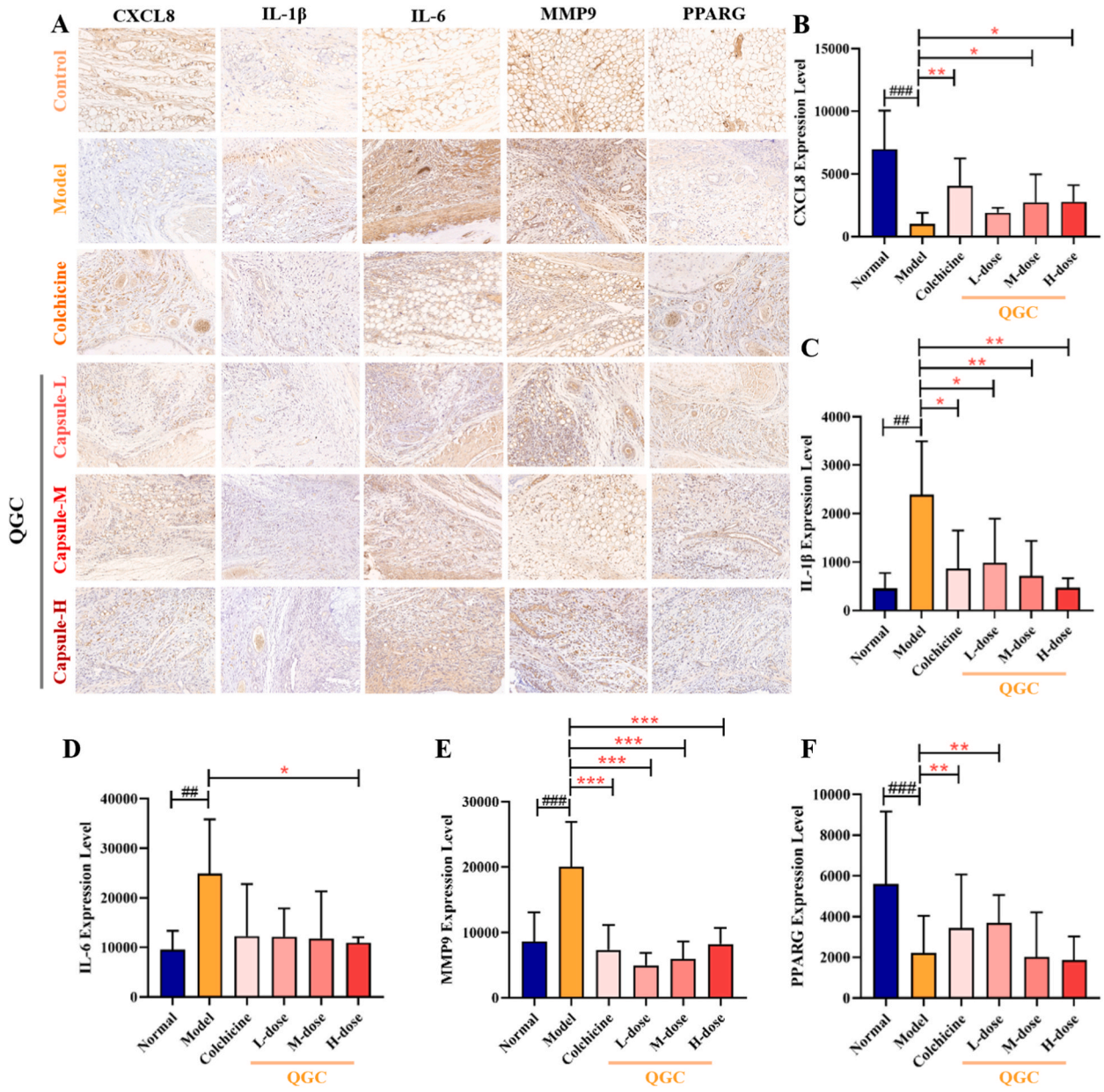

Fig. 10. The protein expression of CXCL8, IL-6, IL-1β, MMP9 and PPARG in the synovial tissue of rats in each treatment group. **(A)** The CXCL8, IL-1β, IL-6, MMP9 and PPARG expressions were detected by immunohistochemistry. The quantitative analysis of **(B)** CXCL8, **(C)** IL-1β, **(D)** IL-6, **(E)** MMP9, and **(F)** PPARG. (n = 3), Compared with the normal group, $^{\#\#}p < 0.01$, $^{\#\#\#}p < 0.001$. Compared with the model group, $^{*}p < 0.05$, $^{**}p < 0.01$.

disease targets. This analysis identified 234 targets, of which 16 key targets were selected for QGC treatment of GA. Further GO and KEGG enrichment analysis indicated that these 16 targets are mainly associated with IL-17, rheumatoid arthritis, MAPK, and PI3K/Akt signaling pathways. The IL-17 pathway has been implicated in anti-inflammatory responses and defense against microbial and inflammatory diseases [40–42].

Activation of the IL-17 family signaling pathway triggers downstream pathways such as NF-κB, MAPK, and C-EBP through specific receptors. This activation leads to the production of antimicrobial peptides, cytokines, and chemokines [43]. The PI3K/Akt pathway serves as a crucial intracellular signal transduction pathway [44]. When binding to growth factor receptors such as EGFR, PI3K can modify Akt proteins' structure and activation, thereby regulating downstream substrates like apoptosis-related proteins Bad and Caspase-9. This regulatory mechanism impacts various cellular processes like apoptosis, proliferation, differentiation, and migration in chondrocytes [45,46]. Furthermore, the PI3K/Akt signaling pathway has the potential to suppress the inflammatory response, possibly by activating the NF-κB pathway [47,48]. The MAPK (mitogen-activated protein kinase) family comprises serine/threonine protein kinases that have been extensively researched for their role in activating cellular autophagy and reducing inflammation *in vivo*,

primarily via the MAPK/NF-κB signaling pathway [48–51]. Building upon these findings, we propose that QGC may aid in the treatment of GA through multiple signaling pathways. To validate the anticipated results of network pharmacology, we utilized molecular docking to simulate the binding affinity of the active ingredients to the targets. The outcomes revealed that the five main active ingredients displayed a strong binding potential to CXCL8, IL-1β, IL-6, MMP9, and PPARG. Li's experiments illustrated that kaempferol could mitigate mechanical abnormal pain, ankle edema, and inflammation in MSU by inhibiting the expression of IL-1β, IL-6, TNF-α, and TGF-β1 while restoring Th17/Treg imbalance [52]. Furthermore, kaempferol demonstrates anti-inflammatory properties by increasing the expression levels of CXCL8 and PPARG and inhibiting NF-kB activation [53,54]. Other studies have shown that lignans can diminish the inflammatory response of GA by suppressing the NF-kB signaling pathway, resulting in significant reductions in IL-1β, IL-6, and TNF-α levels, decreased NF-κB protein levels, and increased expression of the chemokine CXCL8. Xie et al.'s experimental findings revealed that lignans exhibit strong binding to PPARG, leading to a significant upregulation of PPARG expression and inhibition of IL-1β, IL-6, and COX2 expression in inflammatory monocytes [55,56]. Nobiletin activates the AMPK signaling pathway, leading to upregulation of PPARG expression and a significant reduction in macrophage infiltration, resulting in anti-inflammatory effects [57,58]. Another study demonstrated that Nobiletin upregulates PPARG, PPARA, and CXCL8 levels, while inhibiting MMP9 expression and suppressing the release of inflammatory factors TNF-α and IL-6, also achieving anti-inflammatory effects [59]. Quercetin, a common flavonoid constituent, exhibits potent anti-inflammatory activity by acting as a PPARG agonist to reduce MSU-induced inflammation, block NF-kB activation, and down-regulate the production and expression of IL-1β, IL-6, and MMP9 [60–62]. Wogonin effectively inhibits migration, invasion, and production of pro-inflammatory cytokines (TNF-α, IL-1β, IL-6, MMP-3, and MMP-9) in RA fibroblast-like synoviocytes through the PI3K/AKT/NF-κB pathway. Additionally, Wogonin inhibits myofibrillar differentiation of MH7A cells, increases E-calmodulin expression, and decreases α-smooth muscle actin expression, effectively ameliorating joint destruction in mice [63–65]. These findings highlight the importance of these five targets in the therapeutic effects of QGC against GA. Furthermore, a rat model of MSU-induced acute arthritis was established to investigate the therapeutic effects of QGC on GA. Given that GA is an auto-metabolic rheumatic disease characterized by slow resolution of inflammation and high recurrence rates, a novel treatment approach involves inhibiting inflammation development and reducing uric acid concentration in patients.

TNF-α and IL-6 are pro-inflammatory cytokines crucial for mediating the inflammatory response in GA, with elevated levels linked to pain, redness, and warmth. Our study also examined markers of oxidative stress like MDA and SOD, essential in inflammation. Increased MDA levels suggest lipid peroxidation, while decreased SOD levels indicate compromised antioxidative defenses in GA. These oxidative stress changes correlate with inflammation and tissue damage severity, making them valuable GA indicators. Our findings suggest that QGC possesses anti-inflammatory properties by reducing IL-6 and TNF-α secretion, enhancing SOD levels, and decreasing serum MDA levels. Enrichment analysis highlighted the IL-17 signaling pathway as a key focus, with QGC reducing IL-1β, IL-6, and MMP9 expression in ankle synovial tissue, while increasing CXCL8 and PPARG expression. CXCL8, a chemokine, aids in pathogen elimination by binding to CXCR1 and CXCR2 receptors [66]. Interestingly, The unexpected CXCL8 expression pattern observed in our gout arthritis model raises questions about potential underlying mechanisms. The resolution phase of inflammation often involves counter-regulatory processes, potentially explaining the post-treatment increase in CXCL8 and suggesting a homeostatic response to QGC intervention. Activation of alternative inflammatory pathways not typically associated with crystalline-induced responses in GA may contribute to the unique regulation of CXCL8 in our model. The complex nature of the multi-component QGC, including potential dose-dependent effects, offers a pharmacological perspective on the nuanced modulation of CXCL8. These findings highlight the delicate balance of pro- and anti-inflammatory signals in GA pathology, emphasizing the need for further detailed investigation into the specific contributions of these mechanisms to the disease and its treatment. Matrix factors, formed by breaking down proteins in the extracellular matrix, interact with specific receptors to regulate cellular activity, influencing processes such as inflammation, immune response, organ development, and wound repair. These factors play a role in cell migration, chemotaxis, and mitosis. MMPs, enzymes involved in breaking down components of the extracellular matrix, are crucial in both normal physiological conditions and disease. Among the 20 identified MMPs, MMP-1, -2, -8, -9, and -12 regulate matrix factors like elastin peptide and prolyl-glycyl-proline (PGP) [67]. PGP and its acetylated form (Ac-PGP) act as chemoattractants for neutrophils by being produced through collagen degradation, potentially playing a role in chronic inflammatory diseases [68]. In arthritic conditions, MMP-9 can be secreted by synovial cells within joints, along with other matrix metalloproteinases such as matrix metalloproteinase-3 [69,70]. These enzymes degrade non-collagenous matrix components in the joints, ultimately reducing inflammation. Research has indicated a significant correlation between MMP9 and the IL-17 signaling pathway. By enhancing IL-17 signaling pathway transduction, drugs can potentially exhibit anti-inflammatory effects by upregulating the downstream target MMP9 [52,71]. PPARG, a nuclear hormone receptor, is found in many tissue cells and is important for controlling adipose tissue differentiation, metabolism, and protecting bones and joints. Studies show that PPARG can lower the levels of inflammatory markers like IL-1β, IL-6, TNF-α, and certain chemokines (CXCL-1, CXCL-5) triggered by MSU, as well as reduce the amount of inflammatory cells in arthritis [72–74]. In our study, we found that only the low dose of QGC had a significant impact on PPARG expression. This difference can be attributed to three factors. Firstly, the complex dose-response dynamics should be considered, as low doses may have a preference for engaging PPARG, while higher doses could lead to receptor desensitization or activate alternative signaling pathways. Secondly, it is important to take into account pharmacokinetic considerations, as varying doses can greatly affect the bioavailability of QGC and its interaction with PPARG. Lastly, the interactive effects among QGC's active components should not be overlooked. These components may have synergistic or antagonistic properties depending on their concentrations, resulting in different biological effects. In conclusion, our findings suggest that QGC has the ability to modulate IL-17 signaling pathways and exert anti-inflammatory effects on inflammatory conditions (Fig. 11).

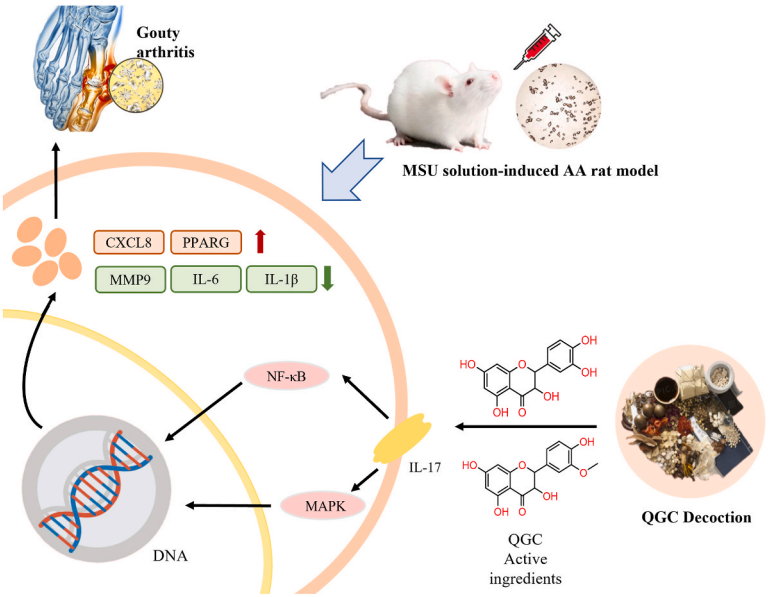

Fig. 11. Diagram of the mechanism of QGC in the treatment of GA.

5. Conclusion

Collectively, we employed UPLC-Q Exactive-MS technology to investigate the pharmacodynamic substances and mechanism of QGC in treating GA. Our analysis identified 39 components, including isorhamnetin, quercetin, and neohesperidin, as potential major chemical compounds responsible for QGC's anti-GA effects. Our study suggests that QGC primarily acts on signaling pathways like IL-17, rheumatoid arthritis, and the MAPK pathway to exert its effects. Molecular docking experiments revealed that the active ingredients in QGC have a strong affinity for therapeutic targets such as CXCL8, IL-1β, IL-6, MMP9, and PPARG, consistent with our network pharmacology analysis. Animal experiments confirmed QGC's anti-inflammatory activity in GA rats, showing protective effects on cartilage and dose-dependent inhibition of inflammation, possibly through the IL-17 signaling pathway. While our initial findings shed light on QGC's active components, further *in vivo* analysis is needed for a deeper understanding. Future experiments, both *in vivo* and *in vitro*, will help determine whether these components act individually or synergistically. Analyzing incoming components through serum pharmacochemistry and utilizing systemic pharmacology, PCR, WB, and gene knockout techniques can refine our understanding of QGC's therapeutic mechanism for GA treatment. Our network analysis also suggests potential associations of QGC's anti-GA effect with rheumatoid arthritis, MAPK, and PI3K/Akt signaling pathways, offering new directions for future research.

Data availability statement

Data supporting the results of this study may be obtained from the corresponding author upon reasonable request.

Ethical approval and consent to participate

All animal experiments were conducted in accordance with the Guidelines for Animal Care and Use (China) and approved by the Ethics Committee of Chengdu University of Traditional Chinese Medicine (Ethical approval number: 2018-15).

CRediT authorship contribution statement

Gelin Xiang: Writing – original draft, Visualization, Investigation, Data curation, Methodology. **Luyin Yang:** Visualization, Investigation, Data curation, Methodology, Writing – original draft. **Jing Qin:** Methodology, Investigation, Data curation. **Shaohui Wang:** Writing – review & editing, Supervision, Conceptualization. **Yi Zhang:** Writing – review & editing, Supervision, Resources, Conceptualization. **Sijin Yang:** Writing – review & editing, Supervision, Resources.

Declaration of competing interest

The authors declare that they have no known competing financial interests or personal relationships that could have appeared to influence the work reported in this paper.

Acknowledgements

This study was supported by projects from Sichuan Administration of traditional Chinese Medicine (2020HJZX004) and Innovation Team, Talents Cultivation Program of National Administration of Traditional Chinese Medicine (ZYYCXTD-C-202207) and Luzhou Municipal Bureau of Science, Technology and Talent Work (Project Number: 2022-RCM-172; Lushi Science and Technology Knowledge [2017] No. 241).

References

[1] E.T. Jia, S.H. He, J.J. Huang, J.Y. Zhang, Research status of sinomenine in the treatment of gouty arthritis, J Guizhou Univ of Tradit Chin Med 44 (3) (2022) 66–70.
[2] H.J. Liu, Y.X. Fan, X.X. Pan, L. Jiang, W.T. Liu, G.Q. Zhang, Experimental research of procyanidine for acute gouty arthritis in rats, Chin J of Mod Drug Appl 10 (22) (2016) 194–196.
[3] W.J. Ye, Y.W. Cheng, X.T. Qiu, Research progress in the treatment of hyperuricemia with traditional Chinese medicine, Hainan Med J 31 (9) (2020) 1187–1190.
[4] F. Rees, M. Hui, M. Doherty, Optimizing current treatment of gout, Nat. Rev. Rheumatol. 10 (5) (2014) 271–283, https://doi.org/10.1038/nrrheum.2014.32.
[5] B.I. Coskun, Are non-steroidal anti-inflammatory drugs safe and effective in patients with acute gout? A cochrane review summary with commentary, Int. J. Rheum. Dis. 26 (6) (2023) 1178–1182, https://doi.org/10.1111/1756-185X.14583.
[6] K.R. Rasheed, R. Shamim, M.S. Sultana, et al., Medicinal plants and nonsteroidal anti-inflammatory drugs (nsaids) in treatment of arthritis: a literature review, Altern. Ther. Health Med. 28 (7) (2022) 58–64.
[7] H. Liang, L. Zhao, J. Yang, X.L. Zhou, C.J. Wang, X.L. Zhou, Research progress in chemical constituents and pharmacological effects of zanthoxylum bungeanum, West China J. Pharm. Sci. 29 (1) (2014) 91–94.
[8] P. Li, Z.H. Hu, Research progress in biology, chemical constituents, and biological activities of rubia cordifolia, Chin. Tradit. Herb. Drugs 44 (14) (2013) 2009–2014.
[9] R. Huang, Y. Yuan, Y. Yuan, et al., Effect of qianhua capsule on symptoms and inflammation in rats with acute gouty arthritis, Chin. Tradit. Pat. Med. 41 (8) (2019) 1973–1976.
[10] R. Huang, J.Y. Xiong, Q.R. Pu, W. Ren, Z.H. Tan, S.J. Yang, Evaluation of the pharmacodynamics of qianhua gout pill in the prevention and treatment of gout based on different animal models, Pharmacol Clin Chin Mater Med 37 (1) (2021) 179–184.
[11] Z. Ding, R. Zhong, Y. Yang, et al., Systems pharmacology reveals the mechanism of activity of ge-gen-qin-lian decoction against lps-induced acute lung injury: a novel strategy for exploring active components and effective mechanism of tcm formulae, Pharmacol. Res. 156 (2020) 104759, https://doi.org/10.1016/j.phrs.2020.104759.
[12] X. Wei, R. Zhou, Y. Chen, et al., Systemic pharmacological verification of baixianfeng decoction regulating tnf-pi3k-akt-nf-kappab pathway in treating rheumatoid arthritis, Bioorganic Chem 119 (2022) 105519, https://doi.org/10.1016/j.bioorg.2021.105519.
[13] A.B. Nair, S. Jacob, A simple practice guide for dose conversion between animals and human, J. Basic Clin. Pharm. 7 (2) (2016) 27–31, https://doi.org/10.4103/0976-0105.177703.
[14] N. Dalbeth, T.R. Merriman, L.K. Stamp, Gout, Lancet 388 (10055) (2016) 2039–2052, https://doi.org/10.1016/S0140-6736(16)00346-9.
[15] A. Scuiller, T. Pascart, A. Bernard, E. Oehler, Rev. Med. Interne 41 (6) (2020) 396–403, https://doi.org/10.1016/j.revmed.2020.02.014 [Gout].
[16] N. Dalbeth, B. Clark, K. Gregory, et al., Mechanisms of bone erosion in gout: a quantitative analysis using plain radiography and computed tomography, Ann. Rheum. Dis. 68 (8) (2009) 1290–1295, https://doi.org/10.1136/ard.2008.094201.
[17] D. Bekaryssova, M. Yessirkepov, K. Mahmudov, Structure, demography, and medico-social characteristics of articular syndrome in rheumatic diseases: a retrospective monocentric analysis of 2019-2021 data, Rheumatol. Int. 43 (11) (2023) 2057–2064, https://doi.org/10.1007/s00296-023-05435-x.
[18] P. Deng, S. Wang, X. Sun, et al., Global trends in research of gouty arthritis over past decade: a bibliometric analysis, Front. Immunol. 13 (2022) 910400, https://doi.org/10.3389/fimmu.2022.910400.
[19] T. Bardin, M.A. Voshaar, M.A. van de Laar, The human and economic burden of difficult-to-treat gouty arthritis, Joint Bone Spine 82 (Suppl 1) (2015) eS2–eS8, https://doi.org/10.1016/S1297-319X(15)30002-6.
[20] N. Schlesinger, N.L. Edwards, P.P. Khanna, A.E. Yeo, P.E. Lipsky, Evaluation of proposed criteria for remission and evidence-based development of criteria for complete response in patients with chronic refractory gout, ACR Open Rheumatol 1 (4) (2019) 236–243, https://doi.org/10.1002/acr2.1025.
[21] N. Dalbeth, J. Collis, K. Gregory, B. Clark, E. Robinson, F.M. Mcqueen, Tophaceous joint disease strongly predicts hand function in patients with gout, Rheumatol 46 (12) (2007) 1804–1807, https://doi.org/10.1093/rheumatology/kem246.
[22] E. Krishnan, Reduced glomerular function and prevalence of gout: nhanes 2009-10, PLoS One 7 (11) (2012) e50046, https://doi.org/10.1371/journal.pone.0050046.
[23] B. Lu, Q. Lu, B. Huang, C. Li, F. Zheng, P. Wang, Risk factors of ultrasound-detected tophi in patients with gout, Clin. Rheumatol. 39 (6) (2020) 1953–1960, https://doi.org/10.1007/s10067-020-04947-2.
[24] S.M. Haftcheshmeh, M. Abedi, K. Mashayekhi, et al., Berberine as a natural modulator of inflammatory signaling pathways in the immune system: focus on nf-kappab, jak/stat, and mapk signaling pathways, Phytother Res. 36 (3) (2022) 1216–1230, https://doi.org/10.1002/ptr.7407.
[25] S. Khan, A. Hussain, F. Attar, et al., A review of the berberine natural polysaccharide nanostructures as potential anticancer and antibacterial agents, Biomed. Pharmacother. 146 (2022) 112531, https://doi.org/10.1016/j.biopha.2021.112531.
[26] J.W. Shou, P.C. Shaw, Therapeutic efficacies of berberine against neurological disorders: an update of pharmacological effects and mechanisms, Cells 11 (5) (2022), https://doi.org/10.3390/cells11050796.
[27] S. Singh, N. Pathak, E. Fatima, A.S. Negi, Plant isoquinoline alkaloids: advances in the chemistry and biology of berberine, Eur. J. Med. Chem. 226 (2021) 113839, https://doi.org/10.1016/j.ejmech.2021.113839.
[28] B. Zhang, L. Wang, X. Ji, et al., Anti-inflammation associated protective mechanism of berberine and its derivatives on attenuating pentylenetetrazole-induced seizures in zebrafish, J. Neuroimmune Pharm. 15 (2) (2020) 309–325, https://doi.org/10.1007/s11481-019-09902-w.
[29] D. Hao, Y. Li, J. Shi, J. Jiang, Baicalin alleviates chronic obstructive pulmonary disease through regulation of hsp72-mediated jnk pathway, Mol. Med. 27 (1) (2021) 53, https://doi.org/10.1186/s10020-021-00309-z.
[30] H. Zhao, C. Li, L. Li, et al., Baicalin alleviates bleomycin-induced pulmonary fibrosis and fibroblast proliferation in rats via the pi3k/akt signaling pathway, Mol. Med. Rep. 21 (6) (2020) 2321–2334, https://doi.org/10.3892/mmr.2020.11046.
[31] T. Zhou, A. Zhang, G. Kuang, et al., Baicalin inhibits the metastasis of highly aggressive breast cancer cells by reversing epithelial-to-mesenchymal transition by targeting beta-catenin signaling, Oncol. Rep. 38 (6) (2017) 3599–3607, https://doi.org/10.3892/or.2017.6011.
[32] J. Liu, Y. Wei, Q. Luo, et al., Baicalin attenuates inflammation in mice with ova-induced asthma by inhibiting nf-kappab and suppressing ccr7/ccl19/ccl21, Int. J. Mol. Med. 38 (5) (2016) 1541–1548, https://doi.org/10.3892/ijmm.2016.2743.
[33] G. Yan, L. Chen, H. Wang, S. Wu, S. Li, X. Wang, Baicalin inhibits lps-induced inflammation in raw264.7 cells through mir-181b/hmgb1/trl4/nf-kappab pathway, Am. J. Transl. Res. 13 (9) (2021) 10127–10141.
[34] M. Yang, X. Zhu, F. Fu, et al., Baicalin ameliorates inflammatory response in a mouse model of rhinosinusitis via regulating the treg/th17 balance, ENT-Ear Nose Throat J. 101 (2_suppl) (2022) 8S–16S, https://doi.org/10.1177/0145561320986058.
[35] S.O. Ekeuku, K.L. Pang, K.Y. Chin, Palmatine as an agent against metabolic syndrome and its related complications: a review, Drug Des. Dev. Ther. 14 (2020) 4963–4974, https://doi.org/10.2147/DDDT.S280520.

[36] X. Rong, J. Xu, Y. Jiang, et al., Citrus peel flavonoid nobiletin alleviates lipopolysaccharide-induced inflammation by activating il-6/stat3/foxo3a-mediated autophagy, Food Funct. 12 (3) (2021) 1305–1317, https://doi.org/10.1039/d0fo02141e.
[37] G.S. Jeong, D.S. Lee, D.C. Kim, et al., Neuroprotective and anti-inflammatory effects of mollugin via up-regulation of heme oxygenase-1 in mouse hippocampal and microglial cells, Eur. J. Pharmacol. 654 (3) (2011) 226–234, https://doi.org/10.1016/j.ejphar.2010.12.027.
[38] J. Li, J.L. Zhang, X.P. Gong, et al., Anti-inflammatory activity of mollugin on dss-induced colitis in mice, Curr. Med. Sci. 40 (5) (2020) 910–916, https://doi.org/10.1007/s11596-020-2262-5.
[39] Z. Wang, M.Y. Li, C. Mi, K.S. Wang, J. Ma, X. Jin, Mollugin has an anti-cancer therapeutic effect by inhibiting tnf-alpha-induced nf-kappab activation, Int. J. Mol. Sci. 18 (8) (2017), https://doi.org/10.3390/ijms18081619.
[40] J.M. Fletcher, B. Moran, A. Petrasca, C.M. Smith, Il-17 in inflammatory skin diseases psoriasis and hidradenitis suppurativa, Clin. Exp. Immunol. 201 (2) (2020) 121–134, https://doi.org/10.1111/cei.13449.
[41] D. Noviello, R. Mager, G. Roda, R.G. Borroni, G. Fiorino, S. Vetrano, The il23-il17 immune axis in the treatment of ulcerative colitis: successes, defeats, and ongoing challenges, Front. Immunol. 12 (2021) 611256, https://doi.org/10.3389/fimmu.2021.611256.
[42] P. Wojdasiewicz, L.A. Poniatowski, D. Szukiewicz, The role of inflammatory and anti-inflammatory cytokines in the pathogenesis of osteoarthritis, Mediat. Inflamm. 2014 (2014) 561459, https://doi.org/10.1155/2014/561459.
[43] C. Gu, L. Wu, X. Li, Il-17 family: cytokines, receptors and signaling, Cytokine 64 (2) (2013) 477–485, https://doi.org/10.1016/j.cyto.2013.07.022.
[44] Q.L. Wang, D.Z. Yang, C. Lv, Anti-inflammatory effects of gambogic acid in murine collagen-induced arthritis through pi3k/akt signaling pathway, Mol. Med. Rep. 17 (3) (2018) 4791–4796, https://doi.org/10.3892/mmr.2018.8389.
[45] M.L. Cho, J.H. Ju, K.W. Kim, et al., Cyclosporine a inhibits il-15-induced il-17 production in cd4+ t cells via down-regulation of pi3k/akt and nf-kappab, Immunol. Lett. 108 (1) (2007) 88–96, https://doi.org/10.1016/j.imlet.2006.11.001.
[46] Q. Jia, W. Cheng, Y. Yue, et al., Cucurbitacin e inhibits tnf-alpha-induced inflammatory cytokine production in human synoviocyte mh7a cells via suppression of pi3k/akt/nf-kappab pathways, Int. Immunopharm. 29 (2) (2015) 884–890, https://doi.org/10.1016/j.intimp.2015.08.026.
[47] S. He, Y. Fu, B. Yan, et al., Curcumol alleviates the inflammation of nucleus pulposus cells via the pi3k/akt/nf-kappab signaling pathway and delays intervertebral disk degeneration, World Neurosurg 155 (2021) e402–e411, https://doi.org/10.1016/j.wneu.2021.08.079.
[48] S.T. Li, Q. Dai, S.X. Zhang, et al., Ulinastatin attenuates lps-induced inflammation in mouse macrophage raw264.7 cells by inhibiting the jnk/nf-kappab signaling pathway and activating the pi3k/akt/nrf2 pathway, Acta Pharmacol. Sin. 39 (8) (2018) 1294–1304, https://doi.org/10.1038/aps.2017.143.
[49] B. Kharwanlang, R. Sharma, Molecular interaction between the glucocorticoid receptor and mapk signaling pathway: a novel link in modulating the anti-inflammatory role of glucocorticoids, Indian J. Biochem. Biophys. 48 (4) (2011) 236–242.
[50] J. Ren, D. Su, L. Li, et al., Anti-inflammatory effects of aureusidin in lps-stimulated raw264.7 macrophages via suppressing nf-kappab and activating ros- and mapks-dependent nrf2/ho-1 signaling pathways, Toxicol. Appl. Pharmacol. 387 (2020) 114846, https://doi.org/10.1016/j.taap.2019.114846.
[51] S. Yang, F. Li, S. Lu, et al., Ginseng root extract attenuates inflammation by inhibiting the mapk/nf-kappab signaling pathway and activating autophagy and p62-nrf2-keap1 signaling in vitro and in vivo, J. Ethnopharmacol. 283 (2022) 114739, https://doi.org/10.1016/j.jep.2021.114739.
[52] N. Li, S. Chen, W. Deng, et al., Kaempferol attenuates gouty arthritis by regulating the balance of th17/treg cells and secretion of il-17, Inflammation 46 (5) (2023) 1901–1916, https://doi.org/10.1007/s10753-023-01849-8.
[53] L.J. Qi, R.Z. Wang, S. Gao, X.J. Chen, X. Zhang, Y.P. Zhang, Molecular mechanisms underlying the effects of bimin kang mixture on allergic rhinitis: network pharmacology and rna sequencing analysis, BioMed Res. Int. 2022 (2022) 7034078, https://doi.org/10.1155/2022/7034078.
[54] Z. Xu, Y. Xie, J. Song, J. Huang, W. Shi, Mechanism of action of a Chinese herbal compound containing quercetin, luteolin, and kaempferol in the treatment of vitiligo based on network pharmacology and experimental verification, Evid.-based Complement Altern. Med 2022 (2022) 7197533, https://doi.org/10.1155/2022/7197533.
[55] R. Shen, L. Ma, Y. Zheng, Anti-inflammatory effects of luteolin on acute gouty arthritis rats via tlr/myd88/nf-kappab pathway, Zhong Nan Da Xue Xue Bao Yi Xue Ban 45 (2) (2020) 115–122, https://doi.org/10.11817/j.issn.1672-7347.2020.190566.
[56] Y. Xie, Z. Lin, J. Zhang, et al., Virtual screening combined with experimental verification reveals the potential mechanism of fuzitang decoction against gouty arthritis, Heliyon 9 (12) (2023) e22650, https://doi.org/10.1016/j.heliyon.2023.e22650.
[57] H. Wang, Q. Tian, R. Zhang, et al., Nobiletin alleviates atherosclerosis by inhibiting lipid uptake via the pparg/cd36 pathway, Lipids Health Dis. 23 (1) (2024) 76, https://doi.org/10.1186/s12944-024-02049-5.
[58] T. Tsuboi, R. Lu, T. Yonezawa, et al., Molecular mechanism for nobiletin to enhance abca1/g1 expression in mouse macrophages, Atherosclerosis 297 (2020) 32–39, https://doi.org/10.1016/j.atherosclerosis.2020.01.024.
[59] L. Yao, X. Zhang, C. Huang, Y. Cai, C.C. Wan, The effect of citrus aurantium on non-small-cell lung cancer: a research based on network and experimental pharmacology, BioMed Res. Int. 2023 (2023) 6407588, https://doi.org/10.1155/2023/6407588.
[60] D. Das, A. Banerjee, S. Mukherjee, B.K. Maji, Quercetin inhibits nf-kb and jak/stat signaling via modulating tlr in thymocytes and splenocytes during msg-induced immunotoxicity: an in vitro approach, Mol. Biol. Rep. 51 (1) (2024) 277, https://doi.org/10.1007/s11033-024-09245-7.
[61] X. Gong, Y. Huang, Q. Ma, M. Jiang, K. Zhan, G. Zhao, Quercetin alleviates lipopolysaccharide-induced cell damage and inflammation via regulation of the tlr4/nf-kappab pathway in bovine intestinal epithelial cells, Curr, Issues Mol. Biol. 44 (11) (2022) 5234–5246, https://doi.org/10.3390/cimb44110356.
[62] W. Jiang, J. Liu, X. Zhao, W. Yang, Combination of network pharmacology and in vitro experiments on lpsinduced a549 cells to explore the molecular mechanisms of huanglian jiedu decoction treating pneumonia, Comb. Chem. High Throughput Screen. 26 (3) (2023) 559–575, https://doi.org/10.2174/1386207325666220421110032.
[63] H. Yang, C. Liu, X. Lin, et al., Wogonin inhibits the migration and invasion of fibroblast-like synoviocytes by targeting pi3k/akt/nf-kappab pathway in rheumatoid arthritis, Arch. Biochem. Biophys. (2024) 109965, https://doi.org/10.1016/j.abb.2024.109965.
[64] J.H. Go, J.D. Wei, J.I. Park, K.S. Ahn, J.H. Kim, Wogonin suppresses the lps-enhanced invasiveness of mda-mb-231 breast cancer cells by inhibiting the 5-lo/blt2 cascade, Int. J. Mol. Med. 42 (4) (2018) 1899–1908, https://doi.org/10.3892/ijmm.2018.3776.
[65] N.M. Khan, A. Haseeb, M.Y. Ansari, P. Devarapalli, S. Haynie, T.M. Haqqi, Wogonin, a plant derived small molecule, exerts potent anti-inflammatory and chondroprotective effects through the activation of ros/erk/nrf2 signaling pathways in human osteoarthritis chondrocytes, Free Radic. Biol. Med. 106 (2017) 288–301, https://doi.org/10.1016/j.freeradbiomed.2017.02.041.
[66] R.C. Russo, C.C. Garcia, M.M. Teixeira, F.A. Amaral, The cxcl8/il-8 chemokine family and its receptors in inflammatory diseases, Expert Rev. Clin. Immunol. 10 (5) (2014) 593–619, https://doi.org/10.1586/1744666X.2014.894886.
[67] J.M. Wells, A. Gaggar, J.E. Blalock, Mmp generated matrikines, Matrix Biol. 44–46 (2015) 122–129, https://doi.org/10.1016/j.matbio.2015.01.016.
[68] N.S. Bondarenko, A.N. Shneiderman, A.A. Guseva, B.A. Umarova, Prolyl-glycyl-proline (pgp) peptide prevents an increase in vascular permeability in inflammation, Acta Naturae 9 (1) (2017) 52–55.
[69] N.I. Medeiros, J. Gomes, R. Correa-Oliveira, Synergic and antagonistic relationship between mmp-2 and mmp-9 with fibrosis and inflammation in chagas' cardiomyopathy, Parasite Immunol. 39 (8) (2017), https://doi.org/10.1111/pim.12446.
[70] X. Wang, Y.Y. Yu, S. Lieu, et al., Mmp9 regulates the cellular response to inflammation after skeletal injury, Bone 52 (1) (2013) 111–119, https://doi.org/10.1016/j.bone.2012.09.018.
[71] S.H. Sun, C.D. Angell, H. Savardekar, et al., Btk inhibition potentiates anti-pd-l1 treatment in murine melanoma: potential role for mdsc modulation in immunotherapy, Cancer Immunol. Immunother. 72 (11) (2023) 3461–3474, https://doi.org/10.1007/s00262-023-03497-1.
[72] R.C. Wang, D.M. Jiang, Ppar-gamma agonist pioglitazone affects rat gouty arthritis by regulating cytokines, Genet. Mol. Res. 13 (3) (2014) 6577–6581, https://doi.org/10.4238/2014.August.28.2.
[73] J. Wang, G. Chen, L. Lu, H. Zou, Sirt1 inhibits gouty arthritis via activating ppargamma, Clin. Rheumatol. 38 (11) (2019) 3235–3242, https://doi.org/10.1007/s10067-019-04697-w.
[74] W.C. Chang, W.Y. Jan, W.H. Chung, et al., Genetic variants of ppar-gamma coactivator 1b augment nlrp3-mediated inflammation in gouty arthritis, RHEUMATOLOGY 56 (3) (2017) 457–466, https://doi.org/10.1093/rheumatology/kew337.

[75] F.B. Vicente, G. Vespa, A. Miller, S. Haymond, Quantification of arginine and its methylated derivatives in plasma by high-performance liquid chromatography tandem mass spectrometry (lc-ms/ms), Methods Mol. Biol. 1378 (2016) 21–30, https://doi.org/10.1007/978-1-4939-3182-8_3.

[76] S.Y. Kim, B.K. Kim, M.R. Gwon, et al., Urinary metabolomic profiling for noninvasive diagnosis of acute t cell-mediated rejection after kidney transplantation, J. Chromatogr. B 1118–1119 (2019) 157–163, https://doi.org/10.1016/j.jchromb.2019.04.047.

[77] W. Yu, C. Xu, G. Li, et al., Simultaneous determination of trimethylamine n-oxide, choline, betaine by uplc-ms/ms in human plasma: an application in acute stroke patients, J. Pharm. Biomed. Anal. 152 (2018) 179–187, https://doi.org/10.1016/j.jpba.2018.01.049.

[78] C. Cheng, Q.Y. Shi, Determination of starch maleate by lc-ms/ms, Cereals Oils Process (4) (2014) 60–62.

[79] X.P. Wen, Q. Peng, F.X. Zou, et al., Simultaneous determination of nine compounds in fruits of quisqualis indica by uplc-ms/ms, Mod Chin Med 22 (11) (2020) 1830–1839.

[80] Y.W. Huang, Y.X. Jin, X. Bao, M.L. Zhang, C.C. Wen, X.Q. Wang, Uplc-ms/ms simultaneous determination of citric acid, succinic acid, fumaric acid, lactic acid, pyruvic acid, malic acid and fructose in rat urine and its applicatio, Strait Pharm J 32 (4) (2020) 33–36.

[81] Z. Wei, Z. Dong, J. Jia, et al., Application of q-tof-ms based metabonomics techniques to analyze the plasma metabolic profile changes on rats following death due to acute intoxication of phorate, Int. J. Legal Med. 135 (4) (2021) 1437–1447, https://doi.org/10.1007/s00414-021-02532-z.

[82] J. Shi, H.F. Liu, J.M. Wong, R.N. Huang, E. Jones, T.J. Carlson, Development of a robust and sensitive lc-ms/ms method for the determination of adenine in plasma of different species and its application to in vivo studies, J. Pharm. Biomed. Anal. 56 (4) (2011) 778–784, https://doi.org/10.1016/j.jpba.2011.07.023.

[83] G.Y. Wang, Determination of cordycepin and adenosine by ultra high performance liquid chromatography-mass spectrometry, Brand & Standardization 1 (2022) 90–92.

[84] B. Noorani, E.A. Chowdhury, F. Alqahtani, et al., Lc-ms/ms-based in vitro and in vivo investigation of blood-brain barrier integrity by simultaneous quantitation of mannitol and sucrose, Fluids Barriers CNS 17 (1) (2020) 61, https://doi.org/10.1186/s12987-020-00224-1.

[85] S. Liang, B. Sanchez-Espiridion, H. Xie, J. Ma, X. Wu, D. Liang, Determination of proline in human serum by a robust lc-ms/ms method: application to identification of human metabolites as candidate biomarkers for esophageal cancer early detection and risk stratification, Biomed. Chromatogr. 29 (4) (2015) 570–577, https://doi.org/10.1002/bmc.3315.

[86] B.L. Li, L.X. Qie, X.G. Wang, L.Y. Niu, Simultaneous determination of fifteen constituents in suanzao anshen granules by uplc-ms/ms, Chin. Tradit. Pat. Med. 44 (6) (2022) 1751–1755.

[87] X. Yang, J.C. Feng, X.L. Xiao, J.G. Wang, T.T. Zhou, S.J. Xiang, Simultaneous determination of maltol, ethyl maltol, vanillin, methyl vanillin and ethyl vanillin in edible vegetable oil by liquid chromatography-mass, China Oils Fats (2022) 1–8.

[88] M. Kuzma, N. Kovacs, L. Sziva, G. Maasz, P. Avar, P. Perjesi, Oxidation of hydroxy- and dihydroxybenzoic acids under the udenfriend's conditions. An hplc study, Open Med. Chem. J. (2018) 13–22, https://doi.org/10.2174/1874104501812010013, 122018.

[89] X.B. Li, F.G. Shi, L.Y. Jian, L. Ding, An lc-ms/ms method for the simultaneous determination of amygdalin and paeoniflorin in human urine and application to urinary excretion study, Acta Pharm. Sin. 50 (10) (2015) 1330–1335.

[90] G. Sagandykova, J. Walczak-Skierska, F. Monedeiro, P. Pomastowski, B. Buszewski, New methodology for the identification of metabolites of saccharides and cyclitols by off-line ec-maldi-tof-ms, Int. J. Mol. Sci. 21 (15) (2020), https://doi.org/10.3390/ijms21155265.

[91] T.L. Ranieri, L.A. Ciolino, Rapid selective screening and determination of ephedrine alkaloids using gc-ms footnote mark, Phytochem. Anal. 19 (2) (2008) 127–135, https://doi.org/10.1002/pca.1025.

[92] S. Deshpande, M.F. Matei, R. Jaiswal, B.S. Bassil, U. Kortz, N. Kuhnert, Synthesis, structure, and tandem mass spectrometric characterization of the diastereomers of quinic acid, J. Agric. Food Chem. 64 (38) (2016) 7298–7306, https://doi.org/10.1021/acs.jafc.6b02472.

[93] D. Szczesny, E. Bartosinska, J. Jacyna, M. Patejko, D. Siluk, R. Kaliszan, Quantitative determination of trigonelline in mouse serum by means of hydrophilic interaction liquid chromatography-ms/ms analysis: application to a pharmacokinetic study, Biomed. Chromatogr. 32 (2) (2018), https://doi.org/10.1002/bmc.4054.

[94] M. Ricciutelli, G. Bartolucci, R. Campana, et al., Quantification of 2- and 3-isopropylmalic acids in forty Italian wines by uhplc-ms/ms triple quadrupole and evaluation of their antimicrobial, antioxidant activities and biocompatibility, Food Chem. 321 (2020) 126726, https://doi.org/10.1016/j.foodchem.2020.126726.

[95] Y. Xiao, Z. Hu, Z. Yin, et al., Profiling and distribution of metabolites of procyanidin b2 in mice by uplc-dad-esi-it-tof-ms(n) technique, Front. Pharmacol. 8 (2017) 231, https://doi.org/10.3389/fphar.2017.00231.

[96] L. Wang, M.S. Halquist, D.H. Sweet, Simultaneous determination of gallic acid and gentisic acid in organic anion transporter expressing cells by liquid chromatography-tandem mass spectrometry, J. Chromatogr. B 937 (2013) 91–96, https://doi.org/10.1016/j.jchromb.2013.08.024.

[97] Y. Chen, X. Cai, G. Li, et al., Chemical constituents of radix actinidia chinensis planch by uplc-qtof-ms, Biomed, Chromatogr 35 (7) (2021) e5103, https://doi.org/10.1002/bmc.5103.

[98] M. Bolechova, J. Caslavsky, M. Pospichalova, P. Kosubova, Uplc-ms/ms method for determination of selected pyrrolizidine alkaloids in feed, Food Chem. 170 (2015) 265–270, https://doi.org/10.1016/j.foodchem.2014.08.072.

[99] Y.P. Su, X.L. Ye, H. Li, W. Xu, K.D. Chu, Simultaneous determination of caffeic acid, protocatechuic acid and chlorogenic acid in gnaphalium affine by uplc-ms/ms, J Int Pharm Res 47 (11) (2020) 1001–1005.

[100] D. Huang, L. Luo, C. Jiang, et al., Sinapine detection in radish taproot using surface desorption atmospheric pressure chemical ionization mass spectrometry, J. Agric. Food Chem. 59 (6) (2011) 2148–2156, https://doi.org/10.1021/jf103725f.

[101] L. Moravsky, B. Michalczuk, B.A. Fateh, P. Papp, A.A. Sysoev, S. Matejcik, Study of atmospheric pressure chemical ionization of phthalates in air by ion mobility spectrometry/mass spectrometry, Rapid Commun. Mass Spectrom. 35 (17) (2021) e9145, https://doi.org/10.1002/rcm.9145.

[102] M. Liu, Stable Isotope Labeling Combined with Lc-Ms for the Quantification of Benzonic Acids in Environment, Dalian University of Technology, 2018, p. 71.

[103] H. Samir, S. Mahgoub, J.M. Badr, A. El-Gendy, G.M. Hadad, E.A. Ibrahim, A uplc- ms/ms method to quantify beta-sitosterol and ferulic acid of pygeum africanum extract in bulk and pharmaceutical preparation, J. Chromatogr. Sci. (2022), https://doi.org/10.1093/chromsci/bmac077.

[104] R. Santockyte, H. Kandoussi, W. Chen, et al., Lc-ms/ms bioanalysis of plasma 1, 14-tetradecanedioic acid and 1, 16-hexadecanedioic acid as candidate biomarkers for organic anion-transporting polypeptide mediated drug-drug interactions, Bioanalysis 10 (18) (2018) 1473–1485, https://doi.org/10.4155/bio-2018-0170.

[105] X. Zhang, P. Li, S. Guo, S. Wang, D. Liu, Quantitation of beta-carboline and quercetin in alligator weed (alternanthera philoxeroides (mart.) Griseb.) by lc-ms/ms and evaluation of cardioprotective effects of the methanol extracts, Drug Discov. Ther. 12 (6) (2018) 341–346, https://doi.org/10.5582/ddt.2018.01070.

[106] A.M. Zaher, A.M. Moharram, R. Davis, P. Panizzi, M.A. Makboul, A.I. Calderon, Characterisation of the metabolites of an antibacterial endophyte botryodiplodia theobromae pat. Of dracaena draco l. By lc-ms/ms, Nat. Prod. Res. 29 (24) (2015) 2275–2281, https://doi.org/10.1080/14786419.2015.1012715.

[107] F.J. Peng, X. Xu, P. Shu, et al., Determination of vanillin and ethyl vanillin contents in beverages by gc and gc——ms, Sci Technol Food Ind 36 (15) (2015) 303–306.

[108] R. Dargue, I. Grant, L.C. Nye, et al., The analysis of acetaminophen (paracetamol) and seven metabolites in rat, pig and human plasma by u(h)plc-ms, Bioanalysis 12 (7) (2020) 485–500, https://doi.org/10.4155/bio-2020-0015.

[109] S. Baba, N. Osakabe, M. Natsume, J. Terao, Orally administered rosmarinic acid is present as the conjugated and/or methylated forms in plasma, and is degraded and metabolized to conjugated forms of caffeic acid, ferulic acid and m-coumaric acid, Life Sci. 75 (2) (2004) 165–178, https://doi.org/10.1016/j.lfs.2003.11.028.

[110] N. Li, C. Liu, S. Mi, et al., Simultaneous determination of oleanolic acid, p-coumaric acid, ferulic acid, kaemperol and quercetin in rat plasma by lc-ms-ms and application to a pharmacokinetic study of oldenlandia diffusa extract in rats, J. Chromatogr. Sci. 50 (10) (2012) 885–892, https://doi.org/10.1093/chromsci/bms086.

[111] Y.Z. Baima, L.Z. Baima, L.M. Yuzhu, C. Ma, Determination of rutin and chlorogenic acid in saussurea involucrata by uhplc-ms/ms, Tibet Sci Technol (8) (2021) 6–9.

[112] Y. Zeng, S. Li, X. Wang, T. Gong, X. Sun, Z. Zhang, Validated lc-ms/ms method for the determination of scopoletin in rat plasma and its application to pharmacokinetic studies, Molecules 20 (10) (2015) 18988–19001, https://doi.org/10.3390/molecules201018988.
[113] B.F. Abu, B.M. Abu, N. Abdullah, S. Endrini, S. Fatmawati, Optimization of extraction conditions of phytochemical compounds and anti-gout activity of euphorbia hirta l. (Ara tanah) using response surface methodology and liquid chromatography-mass spectrometry (lc-ms) analysis, Evid.-based Complement Altern. Med 2020 (2020) 4501261, https://doi.org/10.1155/2020/4501261.
[114] P.Y. Chen, J.W. Yu, F.L. Lu, M.C. Lin, H.F. Cheng, Differentiating parts of cinnamomum cassia using lc-qtof-ms in conjunction with principal component analysis, Biomed. Chromatogr. 30 (9) (2016) 1449–1457, https://doi.org/10.1002/bmc.3703.
[115] B. He, Q. Li, Y. Jia, et al., A uflc-ms/ms method for simultaneous quantitation of spinosin, mangiferin and ferulic acid in rat plasma: application to a comparative pharmacokinetic study in normal and insomnic rats, J. Mass Spectrom. 47 (10) (2012) 1333–1340, https://doi.org/10.1002/jms.3072.
[116] A.L. Santos, M.G. Soares, L.S. de Medeiros, M. Ferreira, P. Sartorelli, Identification of flavonoid-3-o-glycosides from leaves of casearia arborea (salicaceae) by uhplc-dad-esi-hrms/ms combined with molecular networking and nmr, Phytochem. Anal. 32 (6) (2021) 891–898, https://doi.org/10.1002/pca.3032.
[117] X. Liu, Z. Yu, Y. Wang, et al., Therapeutic drug monitoring of polymyxin b by lc-ms/ms in plasma and urine, Bioanalysis 12 (12) (2020) 845–855, https://doi.org/10.4155/bio-2020-0051.
[118] Y.F. Deng, X.J. Zhai, Simultaneous determination of astragulin and kaempferol in bairui granule by hplc-ms/ms, China Pharmacist 21 (3) (2018) 524–526.
[119] A.L. Santos, M.G. Soares, L.S. de Medeiros, M. Ferreira, P. Sartorelli, Identification of flavonoid-3-o-glycosides from leaves of casearia arborea (salicaceae) by uhplc-dad-esi-hrms/ms combined with molecular networking and nmr, Phytochem. Anal. 32 (6) (2021) 891–898, https://doi.org/10.1002/pca.3032.
[120] M. Abbas-Mohammadi, F.M. Moridi, P. Salehi, et al., Molecular networking based dereplication of ache inhibitory compounds from the medicinal plant vincetoxicum funebre (boiss. & kotschy), J. Biomol. Struct. Dyn. 40 (5) (2022) 1942–1951, https://doi.org/10.1080/07391102.2020.1834455.
[121] E. Protasiuk, M. Olejnik, Determination of salicylic acid in feed using lc-ms/ms, J. Vet. Res. 62 (3) (2018) 303–307, https://doi.org/10.2478/jvetres-2018-0044.
[122] J. Yuan, F. Wei, X. Luo, et al., Multi-component comparative pharmacokinetics in rats after oral administration of fructus aurantii extract, naringin, neohesperidin, and naringin-neohesperidin, Front. Pharmacol. 11 (2020) 933, https://doi.org/10.3389/fphar.2020.00933.
[123] W. Zhou, J. Shan, S. Wang, et al., Simultaneous determination of caffeic acid derivatives by uplc-ms/ms in rat plasma and its application in pharmacokinetic study after oral administration of flos lonicerae-fructus forsythiae herb combination, J. Chromatogr. B 949–950 (2014) 7–15, https://doi.org/10.1016/j.jchromb.2013.12.035.
[124] Y. Deng, X. Li, W. Xiao, Z. Wang, Z. Xiong, L. Zhao, Uplc-ms/ms simultaneous determination of seven active ingredients of yaobitong capsule in rat plasma and its integrated pharmacokinetic application, Biomed. Chromatogr. 34 (9) (2020) e4866, https://doi.org/10.1002/bmc.4866.
[125] T.T. Zhang, Y.L. Wang, B. Jin, T. Li, C. Ma, Plasma pharmacokinetics of isorhapontigenin, a novel derivative of stilbenes, in mice by lc-ms/ms method, J. Asian Nat. Prod. Res. 21 (9) (2019) 895–904, https://doi.org/10.1080/10286020.2018.1540602.
[126] P. Hilt, A. Schieber, C. Yildirim, et al., Detection of phloridzin in strawberries (fragaria x ananassa duch.) by hplc-pda-ms/ms and nmr spectroscopy, J. Agric. Food Chem. 51 (10) (2003) 2896–2899, https://doi.org/10.1021/jf021115k.
[127] L.N. Ban, Y.J. Xu, Simultaneous determination of four effective components in shuanghuanglian oral liquid by hplc/ms, Chin. Tradit. Pat. Med. 34 (2) (2012) 265–268.
[128] H. Xie, J. Yang, S. Feng, P. Cheng, J. Zeng, X. Xiong, Simultaneous quantitative determination of sanguinarine, chelerythrine, dihydrosanguinarine and dihydrochelerythrine in chicken by hplc-ms/ms method and its applications to drug residue and pharmacokinetic study, J. Chromatogr. B 985 (2015) 124–130, https://doi.org/10.1016/j.jchromb.2015.01.001.
[129] S.J. Li, Y.Q. Wang, Analysis of serum pharmacochemistry from scutellaria baicalensis based on hplc-q-tof/ms method, Chin. Tradit. Pat. Med. 41 (3) (2019) 595–600.
[130] L. Yang, X. Meng, X. Yu, H. Kuang, Simultaneous determination of anemoside b4, phellodendrine, berberine, palmatine, obakunone, esculin, esculetin in rat plasma by uplc-esi-ms/ms and its application to a comparative pharmacokinetic study in normal and ulcerative colitis rats, J. Pharm. Biomed. Anal. 134 (2017) 43–52, https://doi.org/10.1016/j.jpba.2016.11.021.
[131] H. Zhou, W. Li, L. Sun, W. Li, Q. Liu, A rapid lc-ms/ms method for simultaneous determination of berberine and irbesartan in rat plasma: application to the drug-drug pharmacokinetic interaction study after oral administration in rats, Biomed. Chromatogr. 35 (9) (2021) e5144, https://doi.org/10.1002/bmc.5144.
[132] L.L. Yang, N. Xiao, X.W. Li, et al., Pharmacokinetic comparison between quercetin and quercetin 3-o-beta-glucuronide in rats by uhplc-ms/ms, Sci. Rep. 6 (2016) 35460, https://doi.org/10.1038/srep35460.
[133] H. Liu, C. Xu, W. Wang, Y. Zhao, Development and validation of an lc-esi-ms/ms method for simultaneous determination of ligustroflavone and rhoifolin in rat plasma and its application to a pharmacokinetic study, J. Chromatogr. Sci. 55 (3) (2017) 267–274, https://doi.org/10.1093/chromsci/bmw181.
[134] M. Azizah, P. Pripdeevech, T. Thongkongkaew, C. Mahidol, S. Ruchirawat, P. Kittakoop, Uhplc-esi-qtof-ms/ms-based molecular networking guided isolation and dereplication of antibacterial and antifungal constituents of ventilago denticulata, Antibiotics-Basel 9 (9) (2020), https://doi.org/10.3390/antibiotics9090606.
[135] L.L. Deng, L.H. Yi, L.N. Xu, Y. Wang, Pharmacokinetic study of apigenin, 3-hydroxy-genkwanin and genkwanin in rats after oral administration of extraction of dephne genkwa sieb.et zucc by lc-ms/ms, Chin J Mod Appl Pharm 32 (1) (2015) 54–59.
[136] R. Zheng, H. Xu, W. Wang, R. Zhan, W. Chen, Simultaneous determination of aflatoxin b(1), b(2), g(1), g(2), ochratoxin a, and sterigmatocystin in traditional Chinese medicines by lc-ms-ms, Anal. Bioanal. Chem. 406 (13) (2014) 3031–3039, https://doi.org/10.1007/s00216-014-7750-7.
[137] S. Saha, P.A. Kroon, A simple and rapid lc-ms/ms method for quantification of total daidzein, genistein, and equol in human urine, J. Anal. Methods Chem. 2020 (2020) 2359397, https://doi.org/10.1155/2020/2359397.
[138] A. Huang, H. Xu, R. Zhan, et al., Metabolic profile of skimmianine in rats determined by ultra-performance liquid chromatography coupled with quadrupole time-of-flight tandem mass spectrometry, Molecules 22 (4) (2017), https://doi.org/10.3390/molecules22040489.
[139] Y. Chen, W. Song, Z.H. Peng, B.Y. Ge, F.M. Han, Identification of metabolites of tectoridin in-vivo and in-vitro by liquid chromatography-tandem mass spectrometry, J. Pharm. Pharmacol. 60 (6) (2008) 709–716, https://doi.org/10.1211/jpp.60.6.0005.
[140] X. Chen, L. Xu, S. Guo, et al., Profiling and comparison of the metabolites of diosmetin and diosmin in rat urine, plasma and feces using uhplc-ltq-orbitrap ms (n), J. Chromatogr. B 1124 (2019) 58–71, https://doi.org/10.1016/j.jchromb.2019.05.030.
[141] Y.F. Deng, X.J. Zhai, Simultaneous determination of astragulin and kaempferol in bairui granule by hplc-ms/ms, China Pharm. 21 (3) (2018) 524–526.
[142] Y. Liu, J. Yang, Y.L. Tuo, et al., Hplc-ms/ms determination of quercetin, kaempferol and isorhamnetin in blood and study of pharmacokinetics in rats, China J. Chin. Mater. Med. 40 (19) (2015) 3859–3865.
[143] H. Kataoka, Y. Terada, R. Inoue, K. Mitani, Determination of isophorone in food samples by solid-phase microextraction coupled with gas chromatography-mass spectrometry, J. Chromatogr. A 1155 (1) (2007) 100–104, https://doi.org/10.1016/j.chroma.2007.04.005.
[144] S. Cox, J. Bergman, S. Hawkins, K. Sladky, Development of a method for the determination of hydromorphone in plasma by lc-ms, Biomed. Chromatogr. 32 (12) (2018) e4357, https://doi.org/10.1002/bmc.4357.
[145] Z. Zheng, S. Li, Y. Zhong, et al., Uplc-qtof-ms identification of the chemical constituents in rat plasma and urine after oral administration of rubia cordifolia l. Extract, Molecules 22 (8) (2017), https://doi.org/10.3390/molecules22081327.
[146] B. Nam, H.J. Jang, A.R. Han, et al., Chemical and biological profiles of dendrobium in two different species, their hybrid, and gamma-irradiated mutant lines of the hybrid based on lc-qtof ms and cytotoxicity analysis, Plants-Basel 10 (7) (2021), https://doi.org/10.3390/plants10071376.
[147] X.M. Sun, Q.F. Liao, Y.T. Zhou, X.J. Deng, Z.Y. Xie, Simultaneous determination of borneol and its metabolite in rat plasma by gc-ms and its application to pharmacokinetic study, J. Pharm. Anal. 4 (5) (2014) 345–350, https://doi.org/10.1016/j.jpha.2014.01.005.
[148] J.E. Welke, K.P. Nicolli, K.C. Hernandes, A. Biasoto, C.A. Zini, Adaptation of an olfactometric system in a gc-fid in combination with gcxgc/ms to evaluate odor-active compounds of wine, Food Chem. 370 (2022) 131004, https://doi.org/10.1016/j.foodchem.2021.131004.
[149] M. Agami, R.A. Shaalan, S.F. Belal, M. Ragab, Lc-ms bioanalysis of targeted nasal galantamine bound chitosan nanoparticles in rats' brain homogenate and plasma, Anal. Bioanal. Chem. 413 (20) (2021) 5181–5191, https://doi.org/10.1007/s00216-021-03487-1.

[150] M. Chen, S. Wei, C. Luo, et al., Simultaneous determination of wogonin, oroxylin a, schisandrin, paeoniflorin and emodin in rat serum by hplc-ms/ms and application to pharmacokinetic studies, Biomed. Chromatogr. 31 (10) (2017), https://doi.org/10.1002/bmc.3966.
[151] I.H. Bowen, H.M. Motawe, Isolation and identification of kokusaginine from tinospora malabarica, Planta Med. 51 (6) (1985) 529–530, https://doi.org/10.1055/s-2007-969588.
[152] A. Kumar, V.C. Devaraj, K.C. Giri, S. Giri, S. Rajagopal, R. Mullangi, Development and validation of a highly sensitive lc-ms/ms-esi method for the determination of nobiletin in rat plasma: application to a pharmacokinetic study, Biomed. Chromatogr. 26 (12) (2012) 1464–1471, https://doi.org/10.1002/bmc.2717.
[153] M. Cen, J. Ruan, L. Huang, et al., Simultaneous determination of thirteen flavonoids from xiaobuxin-tang extract using high-performance liquid chromatography coupled with electrospray ionization mass spectrometry, J. Pharm. Biomed. Anal. 115 (2015) 214–224, https://doi.org/10.1016/j.jpba.2015.07.015.
[154] Q. Wu, M. Wang, W.J. Sciarappa, J.E. Simon, Lc/uv/esi-ms analysis of isoflavones in edamame and tofu soybeans, J. Agric. Food Chem. 52 (10) (2004) 2763–2769, https://doi.org/10.1021/jf035053p.
[155] Q. Wang, T. Yan, W. Jiang, et al., Simultaneous quantification of ligustilide, dl-3-n-butylphthalide and senkyunolide a in rat plasma by gc-ms and its application to comparative pharmacokinetic studies of rhizoma chuanxiong extract alone and baizhi chuanxiong decoction, Biomed. Chromatogr. 33 (10) (2019) e4625, https://doi.org/10.1002/bmc.4625.
[156] Z. Ju, X. Tang, Q. Liao, H. Guan, L. Yang, Z. Wang, Pharmacokinetic, bioavailability, and metabolism studies of lusianthridin, a dihydrophenanthrene compound, in rats by liquid chromatography/electrospray ionization tandem mass spectrometry, J. Pharm. Biomed. Anal. 195 (2021) 113836, https://doi.org/10.1016/j.jpba.2020.113836.
[157] D.L. Yue, M.H. Zhou, Q.Z. Li, J.G. Deng, Z.Y. Liu, H.L. Li, Determination of acetophenone in eva products by microwave extraction-gc/ms method, Plastics Science and Technology 39 (3) (2011) 78–80.
[158] L. Liu, Y. Cheng, H. Zhang, Phytochemical analysis of anti-atherogenic constituents of xue-fu-zhu-yu-tang using hplc-dad-esi-ms, Chem. Pharm. Bull. 52 (11) (2004) 1295–1301, https://doi.org/10.1248/cpb.52.1295.
[159] N. Ahmad, M.H. Warsi, Z. Iqbal, M. Samim, F.J. Ahmad, Quantification of curcumin, demethoxycurcumin, and bisdemethoxycurcumin in rodent brain by uhplc/esi-q-tof-ms/ms after intra-nasal administration of curcuminoids loaded pnipam nanoparticles, Drug Test. Anal. 6 (3) (2014) 257–267, https://doi.org/10.1002/dta.1472.
[160] W. Pan, R.F. Zhao, J. Wang, Y. Wang, W. Lei, X.J. Wang, Pharmacokinetic study of curcumin nanoparticles in rats based on uplc-ms/ms analysis technology, Chin. Tradit. Herb. Drugs 47 (21) (2016) 3834–3839.
[161] M. Gao, J. Yang, Z. Wang, et al., Simultaneous determination of purpurin, munjistin and mollugin in rat plasma by ultra high performance liquid chromatography-tandem mass spectrometry: application to a pharmacokinetic study after oral administration of rubia cordifolia l. Extract, Molecules 21 (6) (2016), https://doi.org/10.3390/molecules21060717.
[162] S. Gouveia-Figueira, J. Spath, A.M. Zivkovic, M.L. Nording, Profiling the oxylipin and endocannabinoid metabolome by uplc-esi-ms/ms in human plasma to monitor postprandial inflammation, PLoS One 10 (7) (2015) e0132042, https://doi.org/10.1371/journal.pone.0132042.
[163] X.H. Ren, M.G. Shi, B.N. Liu, J. Shi, Determination of 10 components of morinda officinalis before and after processing by uplc-qqq-ms, J. Chin. Med. Mater. 42 (3) (2019) 588–593.
[164] P.Y. Hu, Y.H. Zhong, J.F. Feng, et al., Pharmacokinetics of five phthalides in volatile oil of ligusticum sinense oliv.cv. Chaxiong, and comparison study on physicochemistry and pharmacokinetics after being formulated into solid dispersion and inclusion compound, BMC Complement. Med. Ther. 21 (1) (2021) 129, https://doi.org/10.1186/s12906-021-03289-z.
[165] J. Li, W. Chen, Y. Wang, H. Yin, An lc-ms/ms method for simultaneous quantification of 11 components of xian-xiong-gu-kang in the plasma of osteoarthritic rats and pharmacokinetic analysis, J. Sep. Sci. 44 (18) (2021) 3386–3397, https://doi.org/10.1002/jssc.202100132.
[166] D. Sun, Q. Yan, X. Xu, et al., Lc-ms/ms analysis and evaluation of the anti-inflammatory activity of components from bushenhuoxue decoction, Pharm. Biol. 55 (1) (2017) 937–945, https://doi.org/10.1080/13880209.2017.1285327.
[167] A.V. Pinto, V.F. Ferreira, L.C. Coutada, [Synthesis of xyloidone and lapachone analogs], An. Acad. Bras. Cienc. 52 (3) (1980) 477–479.
[168] Y. Ishii, K. Nakamura, T. Mitsumoto, et al., Visualization of the distribution of anthraquinone components from madder roots in rat kidneys by desorption electrospray ionization-time-of-flight mass spectrometry imaging, Food Chem. Toxicol. 161 (2022) 112851, https://doi.org/10.1016/j.fct.2022.112851.
[169] G.F. Zhu, C.Y. Jiang, J.T. Wang, L. Tang, Qualitative analysis of jiang-xue-qing alcohol extract chemical components using uplc-q-tof-mse technology combined with unifi database, Guangdong Chemical Industry 47 (20) (2020) 36–38.
[170] L. Zhang, Z.F. Pi, Y.X. Sun, et al., Tandem mass spectrometry study on the in vitro percutaneous permeation characteristics of imperatorin and isoimperatorin from angelica dahurica, J. Chin. Mass Spectrom. Soc. 38 (1) (2017) 37–44.
[171] N. Shende, A. Karale, P. Marathe, S. Chakraborty, A.D. Mallya, R.M. Dhere, Quantitation of residual sodium dodecyl sulfate in meningococcal polysaccharide by gas chromatography-mass spectrometry, Biologicals 60 (2019) 68–74, https://doi.org/10.1016/j.biologicals.2019.05.001.
[172] Z.M. Qin, Y.H. Li, Y.F. Tan, H.L. Li, Determination of nootkatone in rat plasma by lc-tandem mass spectrometry and its application in a pharmacokinetic study, Biomed. Chromatogr. 35 (12) (2021) e5197, https://doi.org/10.1002/bmc.5197.
[173] Y. Xu, K. Huang, Y. Pan, et al., A rapid uflc-ms/ms method for simultaneous determination of formononetin, cryptotanshinone, tanshinone iia and emodin in rat plasma and its application to a pharmacokinetic study of bu shen huo xue formula, J. Chromatogr. B 932 (2013) 92–99, https://doi.org/10.1016/j.jchromb.2013.06.011.
[174] Y.T. Wu, L.C. Lin, T.H. Tsai, Simultaneous determination of honokiol and magnolol in magnolia officinalis by liquid chromatography with tandem mass spectrometric detection, Biomed. Chromatogr. 20 (10) (2006) 1076–1081, https://doi.org/10.1002/bmc.644.
[175] Y. He, Y. Zhang, J. Lu, R. Lin, Isolation and structural elucidation of abietic acid as the main adulterant in an herbal drug for the treatment of psoriasis, J. Pharm. Biomed. Anal. 66 (2012) 345–348, https://doi.org/10.1016/j.jpba.2012.03.007.
[176] W.Q. He, W.S. Lv, Y. Zhang, et al., Study on pharmacokinetics of three preparations from levistolide a by lc-ms-ms, J. Chromatogr. Sci. 53 (8) (2015) 1265–1273, https://doi.org/10.1093/chromsci/bmu224.
[177] M.N. Sastry, S. Claessens, P. Habonimana, N. De Kimpe, Synthesis of the natural products 3-hydroxymollugin and 3-methoxymollugin, J. Org. Chem. 75 (7) (2010) 2274–2280, https://doi.org/10.1021/jo100024b.
[178] S. Gouveia-Figueira, J. Spath, A.M. Zivkovic, M.L. Nording, Profiling the oxylipin and endocannabinoid metabolome by uplc-esi-ms/ms in human plasma to monitor postprandial inflammation, PLoS One 10 (7) (2015) e0132042, https://doi.org/10.1371/journal.pone.0132042.
[179] J. Palandra, J. Prusakiewicz, J.S. Ozer, Y. Zhang, T.G. Heath, Endogenous ethanolamide analysis in human plasma using hplc tandem ms with electrospray ionization, J. Chromatogr. B 877 (22) (2009) 2052–2060, https://doi.org/10.1016/j.jchromb.2009.05.043.
[180] Y. Gu, X.Z. Shi, S.M. Zhao, Q. Gu, X. Lu, G.W. Xu, Determination of arachidonic acid and its metabolites in mouse tissues by high performance liquid chromatography electrospray tandem quadrupole mass spectrometry, Chin. J. Anal. Chem. 38 (8) (2010) 1089–1094.
[181] T. Sharma, S. Jana, A validated lc-ms/ms method for simultaneous determination of 3-o-acetyl-11-keto-beta-boswellic acid (akba) and its active metabolite acetyl-11-hydroxy-beta-boswellic acid (ac-11-oh-ba) in rat plasma: application to a pharmacokinetic study, J. Chromatogr. Sci. 58 (6) (2020) 485–493, https://doi.org/10.1093/chromsci/bmaa010.
[182] S.Y. Lee, J.H. Jeong, B.N. Kim, S.J. Park, Y.C. Park, G.Y. Lee, Lc-ms/ms analysis of puerarin and 18beta-glycyrrhetinic acid in human plasma after oral administration of samso-eum and its application to pharmacokinetic study, Biomed. Chromatogr. 34 (4) (2020) e4774, https://doi.org/10.1002/bmc.4774.
[183] S. Gouveia-Figueira, M.L. Nording, Development and validation of a sensitive uplc-esi-ms/ms method for the simultaneous quantification of 15 endocannabinoids and related compounds in milk and other biofluids, Anal. Chem. 86 (2) (2014) 1186–1195, https://doi.org/10.1021/ac403352e.
[184] J. Palandra, J. Prusakiewicz, J.S. Ozer, Y. Zhang, T.G. Heath, Endogenous ethanolamide analysis in human plasma using hplc tandem ms with electrospray ionization, J. Chromatogr. B 877 (22) (2009) 2052–2060, https://doi.org/10.1016/j.jchromb.2009.05.043.

[185] F.Y. Wang, W.S. Lv, L. Han, Determination and pharmacokinetic study of pachymic acid by lc-ms/ms, Biol. Pharm. Bull. 38 (9) (2015) 1337–1344, https://doi.org/10.1248/bpb.b15-00121.
[186] M. Han, G. Yang, Q. Lin, Y. Yang, H. Zhang, Y. Su, Determination of endogenous bufalin in serum of patients with hepatocellular carcinoma based on hplc-ms/ms, Front. Oncol. 9 (2019) 1572, https://doi.org/10.3389/fonc.2019.01572.
[187] X.L. Pu, K. Xie, J. Cui, Analysis of lipophilic components before and after fried charcoal of Mongolian medicine azei by gas chromatography-mass spectrometry, Lishizhen Med Mater Med Res 20 (8) (2009) 1848–1849.
[188] H.J. Wang, F.J. Liu, C.J. Sha, G.Y. Leng, W.H. Liu, C.N. You, Study on pharmacokinetics and pharmacodynamics of leuprorelin acetate and endogenous testosterone in rats by hplc-ms/ms, Chin J New Drugs 29 (13) (2020) 1549–1555.
[189] D. Bakir, M. Akdeniz, A. Ertas, et al., A gc-ms method validation for quantitative investigation of some chemical markers in salvia hypargeia fisch. & c.a. Mey. Of Turkey: enzyme inhibitory potential of ferruginol, J. Food Biochem. 44 (9) (2020) e13350, https://doi.org/10.1111/jfbc.13350.
[190] Z. Wang, S.M. Zhao, G.Z. Zeng, N.H. Tan, [Chemical constituents from roots and rhizomes of rubia oncotricha and their cytotoxic activities], China J. Chin. Mater. Med. 43 (22) (2018) 4462–4468, https://doi.org/10.19540/j.cnki.cjcmm.2018.0119.
[191] B. Kalaska, M. Ciborowski, T. Domaniewski, et al., Serum metabolic fingerprinting after exposure of rats to quinolinic acid, J. Pharm. Biomed. Anal. 131 (2016) 175–182, https://doi.org/10.1016/j.jpba.2016.08.024.
[192] H. Samir, S. Mahgoub, J.M. Badr, A. El-Gendy, G.M. Hadad, E.A. Ibrahim, A uplc- ms/ms method to quantify beta-sitosterol and ferulic acid of pygeum africanum extract in bulk and pharmaceutical preparation, J. Chromatogr. Sci. (2022), https://doi.org/10.1093/chromsci/bmac077.
[193] J. Pinguet, N. Kerckhove, T. Eljezi, et al., New spe-lc-ms/ms method for the simultaneous determination in urine of 22 metabolites of dehp and alternative plasticizers from pvc medical devices, Talanta 198 (2019) 377–389, https://doi.org/10.1016/j.talanta.2019.01.115.
[194] L.N. Liu, Y.L. Li, H.Y. Jin, K. Zan, S.C. Ma, Study on the determination of five kinds of ginkgolic acid in ginkgo biloba leaves by ultra high performance liquid chromatography-triple quadrupole tandem mass spectrometry, Chin Pharm J 56 (20) (2021) 1684–1689.
[195] M. Luginbuhl, A. Schrock, S. Konig, S. Schurch, W. Weinmann, Determination of fatty acid ethyl esters in dried blood spots by lc-ms/ms as markers for ethanol intake: application in a drinking study, Anal. Bioanal. Chem. 408 (13) (2016) 3503–3509, https://doi.org/10.1007/s00216-016-9426-y.
[196] J.C. Ho, C.M. Chen, L.C. Row, Oleanane-type triterpenes from the flowers, pith, leaves, and fruit of tetrapanax papyriferus, Phytochemistry 68 (5) (2007) 631–635, https://doi.org/10.1016/j.phytochem.2006.10.007.
[197] M. Nestola, A. Thellmann, Determination of vitamins d2 and d3 in selected food matrices by online high-performance liquid chromatography-gas chromatography-mass spectrometry (hplc-gc-ms), Anal. Bioanal. Chem. 407 (1) (2015) 297–308, https://doi.org/10.1007/s00216-014-8123-y.